ESPOO 2004 VTT RESEARCH NOTES 2273

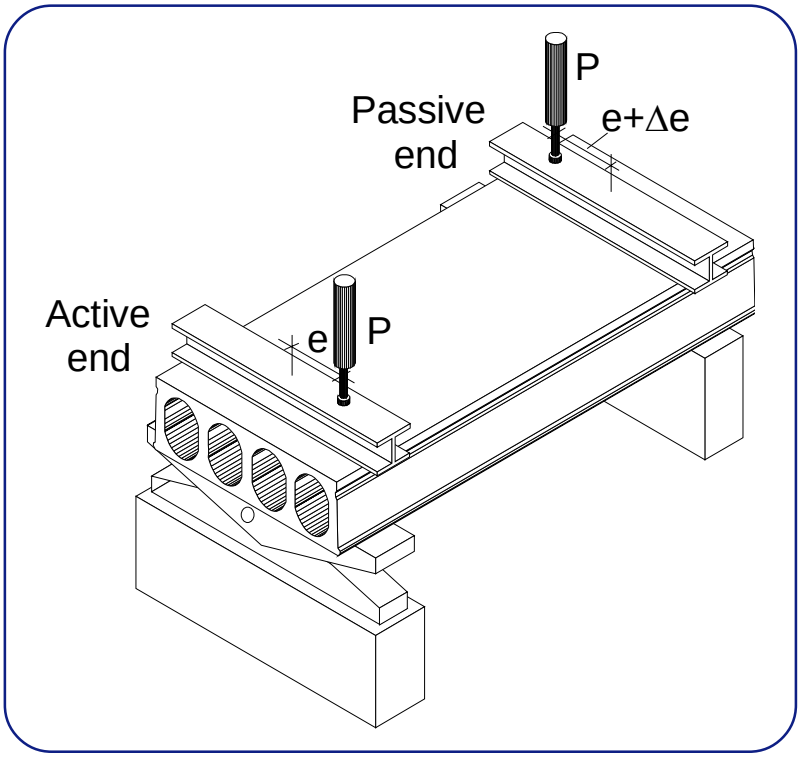

Matti Pajari

Pure torsion tests on single hollow core slabs

VTT TIEDOTTEITA – RESEARCH NOTES 2273

Pure torsion tests on single hollow core slabs

Matti Pajari
VTT Building and Transport

ISBN 951–38–6517–7 (URL: http://www.vtt.fi/inf/pdf/)
ISSN 1455–0865 (URL: http://www.vtt.fi/inf/pdf/)

JULKAISIJA – UTGIVARE – PUBLISHER

VTT, Vuorimiehentie 5, PL 2000, 02044 VTT
puh. vaihde (09) 4561, faksi (09) 456 4374

VTT, Bergsmansvägen 5, PB 2000, 02044 VTT
tel. växel (09) 4561, fax (09) 456 4374

VTT Technical Research Centre of Finland, Vuorimiehentie 5, P.O.Box 2000, FIN–02044 VTT, Finland
phone internat. + 358 9 4561, fax + 358 9 456 4374

VTT Rakennus- ja yhdyskuntatekniikka, Kemistintie 3, PL 1805, 02044 VTT
puh. vaihde 020 722 111, faksi 020 722 7007

VTT Bygg och transport, Kemistvägen 3, PB 1805, 02044 VTT
tel. växel 020 722 111, fax 020 722 7007

VTT Building and Transport, Kemistintie 3, P.O.Box 1805, FIN–02044 VTT, Finland
phone internat. +358 20 722 111, fax +358 20 722 7007

Technical editing Leena Ukskoski

Pajari, Matti. Pure torsion tests on single hollow core slabs. Espoo 2004. VTT Tiedotteita – Research Notes 2273. 29 p. + app. 28 p.

Keywords shear tests, torsion tests, hollow core slabs, testing, test specimens, load testing, failure loads, concrete, precast, prestressed, structure

Abstract

Four tests on prestressed hollow core slab units were carried out. The slab units, two of them 200 mm and two 400 mm in thickness, were subjected to pure torsion. In all tests the observed failure mode was the same as the predicted one, i.e. cracking of top flange in angle of 45º with the longitudinal axis of the slab unit. Although the failure mode was abrupt, the slab units showed considerable ductility after the failure. None of them collapsed before the test had to be interrupted due to excessive rotation.

For 400 mm slabs the torsional stiffness observed in the tests was close to that predicted by elementary calculation method, but for 200 mm slabs the predicted stiffness was 30% lower than that observed. The predicted torsional resistance was 60% and 70% of the observed resistance for 200 mm and 400 mm slabs, respectively, when the lower characteristic value for the tensile strength of the concrete was used for prediction.

Preface

In 2002–2004, a European research project named HOLCOTORS was carried out. It aimed at providing numerical methods for analysis and simplified methods for design of prestressed hollow core floors subjected to shear and torsion. The calculation models were developed by Chalmers University of Technology, Sweden. The tests used for verification of the models were carried out and documented by VTT, Finland. The researchers in the involved research institutes were

Helen Broo	Chalmers
Björn Engström	Chalmers
Karin Lundgren	Chalmers
Matti Pajari	VTT
Mario Plos	Chalmers.

In addition to the researchers, the following representatives of the industrial partners participated in the work as members of the steering group and by participating in the workshops organised on the day before the steering group meetings:

Olli Korander	Consolis Technology, Finland, Chairman
Arnold van Acker	Belgium
Willem Bekker	Echo, Belgium
David Fernandez-Ordonez	Castelo, Spain
Ronald Klein-Holte	BVSH (VBI) The Netherlands
Gösta Lindström	Strängbetong, Sweden
Aad van Paassen	BVSH (VBI), The Netherlands
Nordy Robbens	Echo, Belgium
Bart Thijs	Echo, Belgium
Jan de Wit	IPHA (Dycore), The Netherlands
Javier Zubia	Castelo, Spain.

Gösta Lindström also worked in close co-operation with the researchers, participated in extra workshops between the steering group meetings and made proposals for the future design practice.

The experimental part of the research project, a part of which is documented in this report, was financed by the Fifth Framework Programme of European Commission (Competitive and Sustainable Growth, Contract Nº G6RD-CT-2001-00641); International Prestressed Hollow Core Association, Bundesverband Spannbeton-Hohlplatten, Castelo, Consolis, Echo, Strängbetong, and VTT. The test specimens were provided by Parma Betonila, Finland.

Contents

1. Introduction

The tests documented in this report were planned to represent pure torsion without bending moment, shear force or contribution from neighbouring slab units. The results will mainly be used for calibration of numerical calculation methods. They also give a lower limit for the maximum angle of twist and torque when an isolated slab unit is twisted. This limit is, however, very conservative due to the test arrangements: the cantilevered slab ends and lack of imposed load on the slab increase the tensile stresses in the critical top flange of the slab element, which results in a failure in the top flange. This is not typical of ordinary load cases in which the imposed load on the slab unit reduces the tensile stresses in the top flange and the failure may take place in the webs at a greater torque.

In all figures of this report, the measures are given in millimetres unless otherwise specified.

2. Test arrangements

Four tests on single slab units were carried out in June 2002. Some characteristics of the test specimens are given in Table 1.

Table 1. Characteristics of test specimens.

Test	Thickness mm	Strands	Initial prestress MPa	Length m	Cast	Loaded
PT200A	200	7 d 12.5	900	5.0	23.5.	12.6.
PT200B	200	7 d 12.5	900	5.0	23.5.	17.6.
PT400A	400	7 d 12.5	1000	7.0	24.5.	17.6.
PT400B	400	7 d 12.5	1000	7.0	24.5.	18.6.

The nominal cross-section of the slabs is given in Figs 1 and 2 and the measured geometry in Appendix B. For the shape of the hollow cores see also Fig. 21.

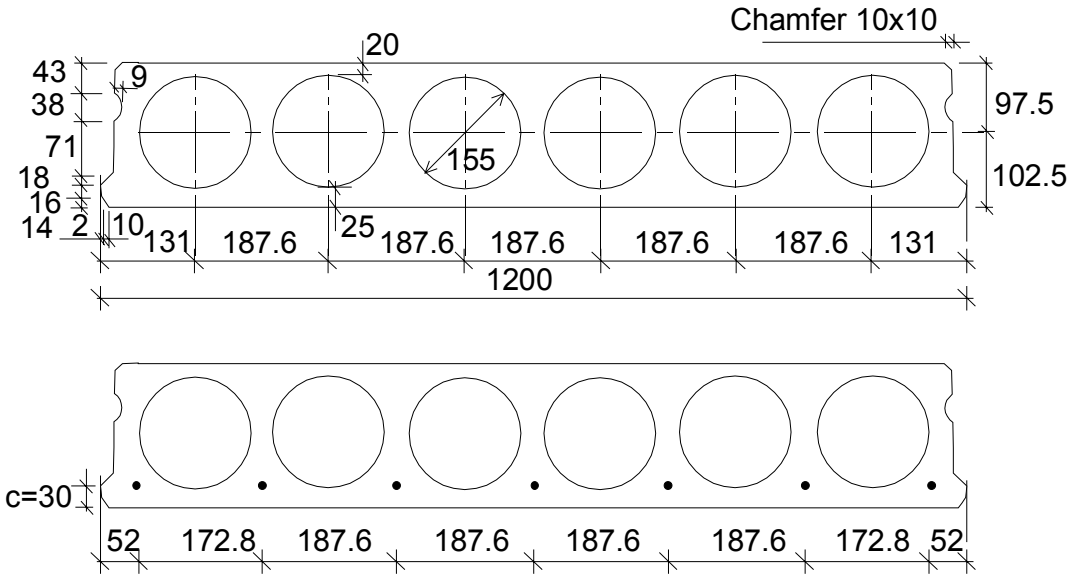

Fig. 1. Nominal cross-section and location of strands in test specimens PT200A and PT200B. c refers to concrete cover below the strand.

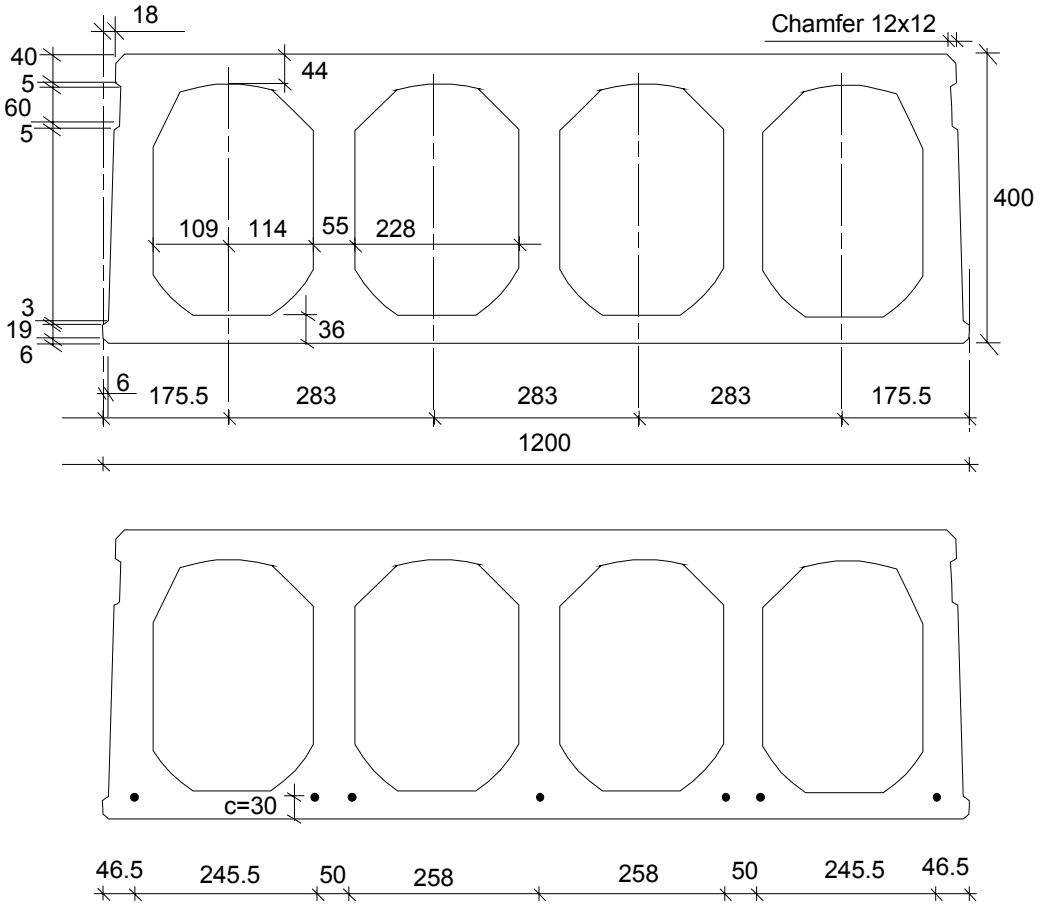

Fig. 2. Nominal cross-section and location of strands in test specimens PT400A and PT400B. c refers to concrete cover below the strand.

The support conditions and loading arrangements are roughly presented in Fig. 3 and in more detail in Figs 4–9. The active end of the slab was free to rotate around an axis parallel to the longitudinal axis of the slab when the slab was in its initial position. Since this rotation axis was located lower than the centroid of the slab cross-section, the rotation was accompanied by longitudinal and lateral displacements of the same order as the vertical displacement. In other words, in addition to the deformation, the slab was subjected to a rigid body motion. Special attention was paid to allow such a motion without additional restraining forces.

At the passive end the support was able to move longitudinally. Thanks to the separate rollers, see Figs 3 and 4 in Appendix A, the passive support was also free to rotate around a vertical axis until an angle of 50 mm / 1200 mm. At the active end the restraints against rotation around a vertical axis (more exactly, axis perpendicular to the steel support) were eliminated by teflon sheets between the steel support and the neoprene strip supporting the slab end, see Figs 8–10 and Appendix A, Fig. 2. Two steel studs welded to the steel support prevented the centroid of the teflon and neoprene strip, and hence also the centroid of the slab end, from sliding relative to the centroid of the support.

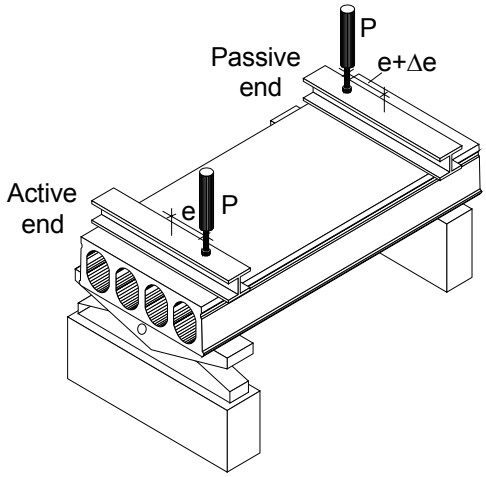

Fig. 3. General view on loading arrangements.

The slab was loaded by two equal point loads at opposite sides of the centreline of the slab. To stabilize the specimen, the load at the passive end had a slightly greater eccentricity than that at the active end.

The detailed arrangements at supports as well as location of the loads and measuring devices are illustrated in Figs 4–8 and in Appendix A, Figs 1–6. The vertical displacement of the slabs were measured by eight transducers 1–8 which were fixed to the floor of the laboratory. The number of the transducers was redundant in order to guarantee recording of rotation in case of malfunction of one transducer.

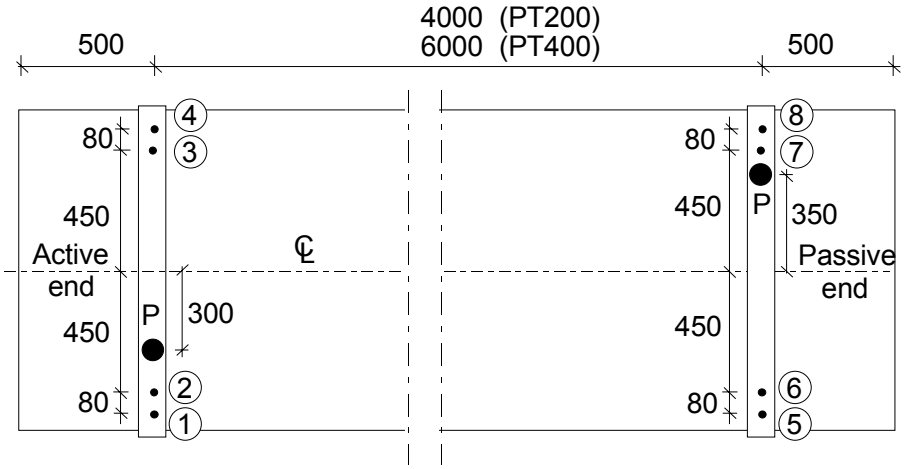

Fig. 4. Top view on test setup.

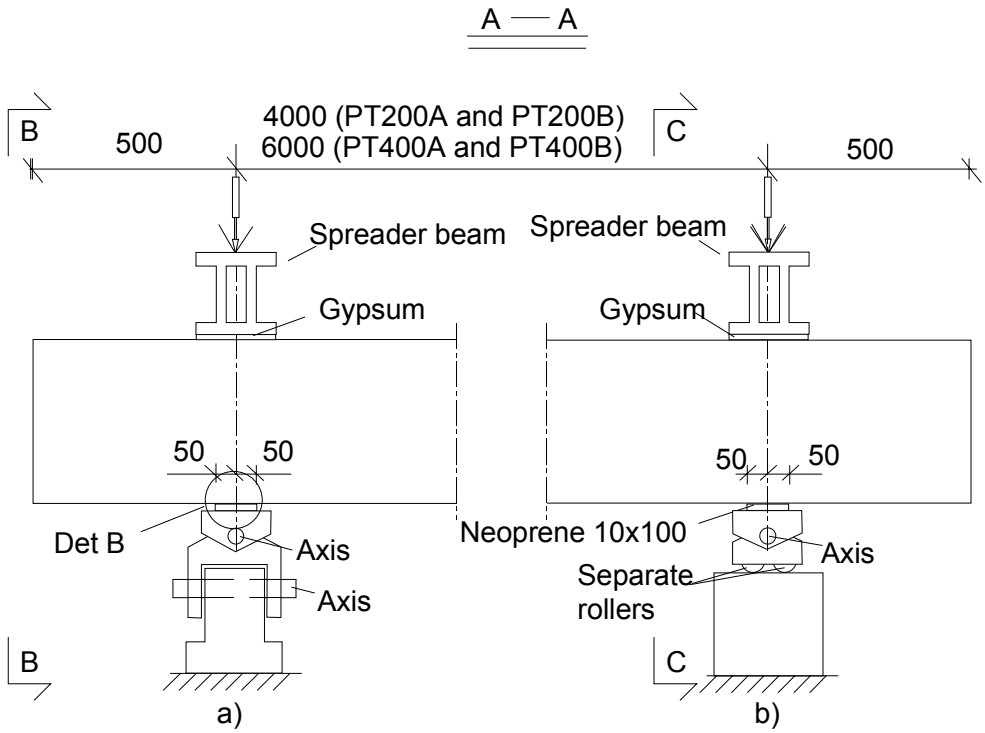

Fig. 5. Side view on test setup. For det B see Fig. 10.

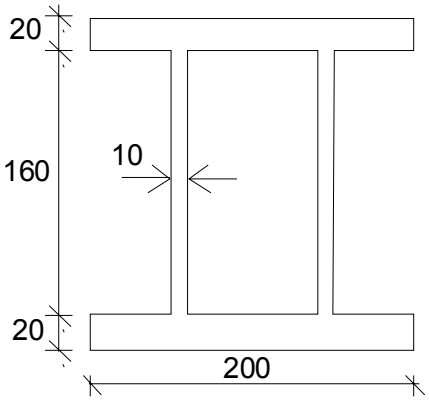

Fig. 6. Cross-section of spreader beam made of steel.

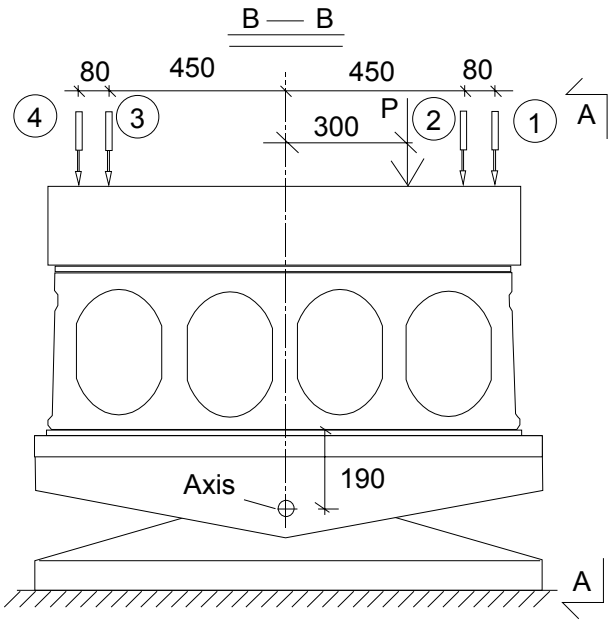

Fig. 7. Active end.

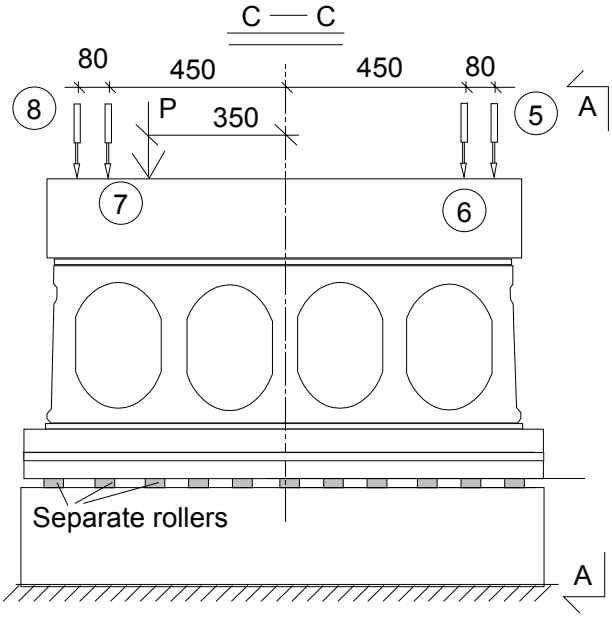

Fig. 8. Passive end.

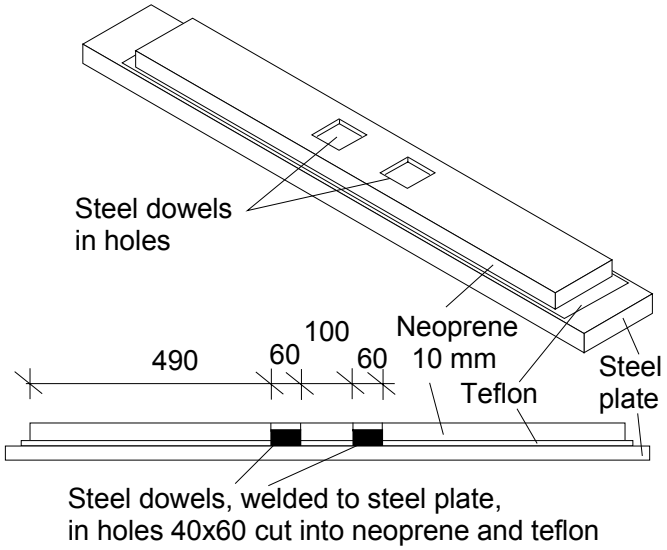

Fig. 9. Support at active end.

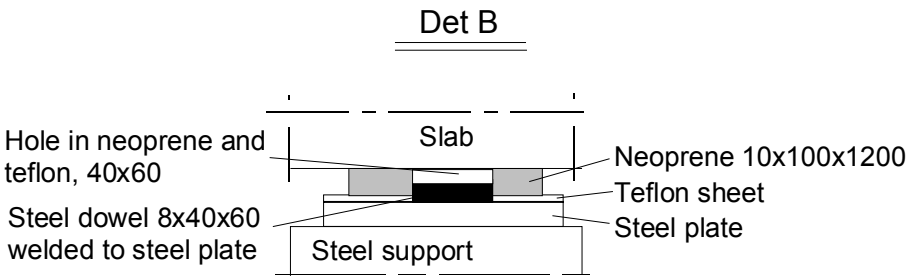

Fig. 10. Detail of support at active end.

3. Loading strategy

The tests were carried out under displacement control. The aimed stages were as follows.

1. Unlock the wedges at the active end, see wedges locked and unlocked in Figs 2 and 6 in App. A, respectively. Zero balance the transducers.
2. Increase the loads until half of the estimated maximum load.
3. Reduce the loads close to zero.
4. After 3 load cycles of the type described in steps 2 and 3 increase the deformation until failure and beyond it as far as possible.

The elongation of the actuator at the active end was used to control the displacements. Attempts were made to keep the rate of elongation piecewise as constant as possible. The actual loading history is illustrated in App. D.

4. Test results

4.1 Failure mode and torque vs. rotation relationship

The failure modes in different tests are illustrated roughly in Fig. 11 and in detail in App. A. In all tests the first cracks appeared on the top of the slab unit at an angle of 45º with the longitudinal axis of the slab. This happening was followed by an abrupt and permanent reduction in torque, i.e. the failure took place at the same time as the first cracking.

The failure of 200 mm and 400 mm slabs took place at the passive and at the active end, respectively. No reason for this difference could be detected. A failure close to the support was more likely than a failure in the span where the bending moment due to the weight of the slab unit reduced the maximum principal stress in the top flange. In addition, the support conditions always create some local disturbance in the stress field, which may facilitate the failure at support. It can be concluded that the failure mode was in all tests exactly what was expected from the theoretical point of view.

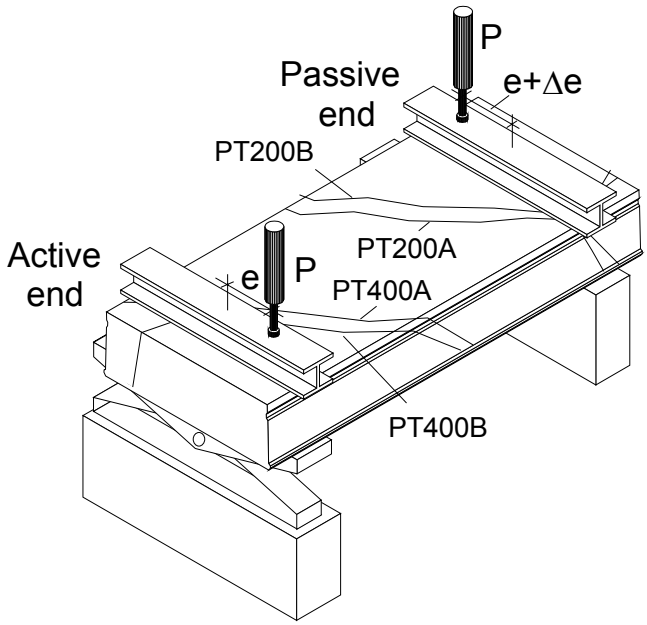

Fig. 11. Failure mode in tests.

For 200 mm slabs the post-cracking torsional resistance was roughly 50%, for 400 mm slab roughly 40% of the maximum resistance. Later on the torque decreased with increasing rotation but there was no collapse. The tests were interrupted due to excessive rotation.

The ductility observed in the tests can be attributed to the prestressed bottom layer of the slab units. In a floor comprising several slab units this means that after the first cracking a slab unit can still participate in the the load-carrying mechanism.

Figs 11–19 illustrate the torque vs. rotation relationship observed in the tests. The torque means the real torque calculated taking into account the displacement of the loaded point at the active end and effect of this displacement on the eccentricity of the couple at the active end as explained in App. C. The rotation means the net rotation (angle of twist) between the line supports, i.e. the rotation measured at the active end minus the rotation measured at the passsive end. It is calculated from expression

$$\phi = \frac{w_1 - w_4 - w_5 + w_8}{1060\ \text{mm}} \tag{1}$$

where w_i is the vertical displacement measured by transducer i, see Fig. 4.

The measured net rotation defined as above represents the angle of twist. After cracking, it reflects the differential rotation of the two separate pieces of slab unit, i.e. it represents rather relative rigid body motion rather than deformation in the slab unit.

Figs 12–14 represent the cyclic loading phase. During the first test PT200A, at the beginning of stage 2, the load increased uncontrolled until 100 kN. To have a better control, an additional valve was installed in the hydraulic circuit and the active end was unlocked only after a small increase of load. Thanks to these arrangements, no problems in the later tests occurred in the automatic control. However, there were problems of other type during test PT200B. The hydraulic pump could not maintain the aimed pressure after the cyclic stage. Due to this, there was an unintended unloading and reloading stage after the intended cyclic stage but before cracking. This can clearly be seen in Fig. 13.

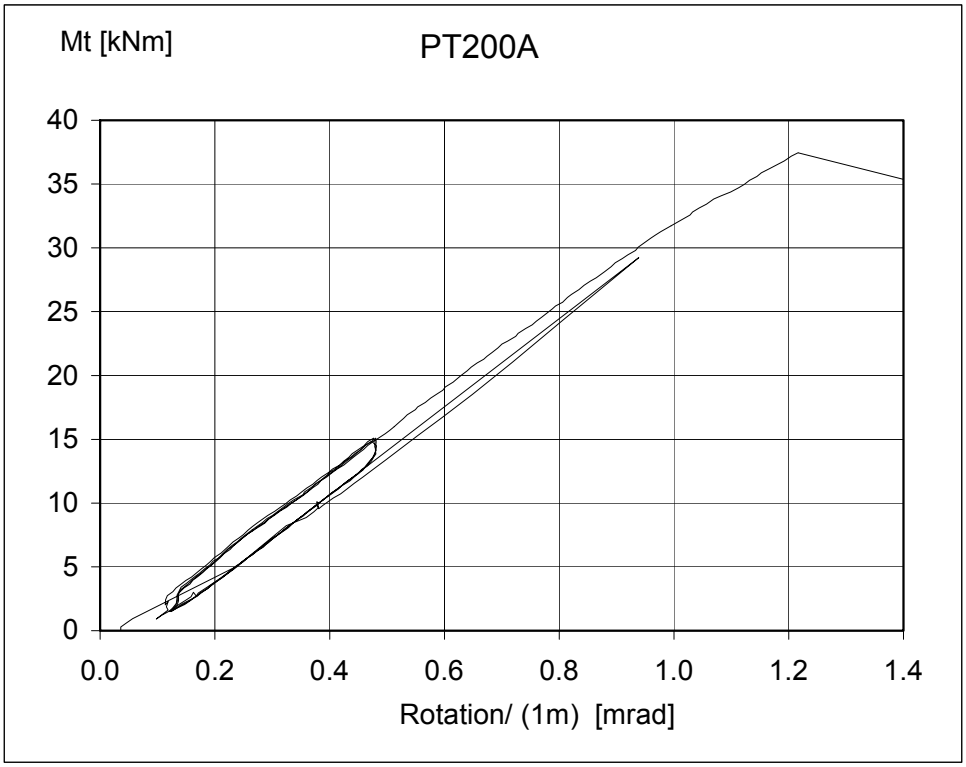

Fig. 12. PT200A. Interdependence of torque and relative angle of twist until cracking.

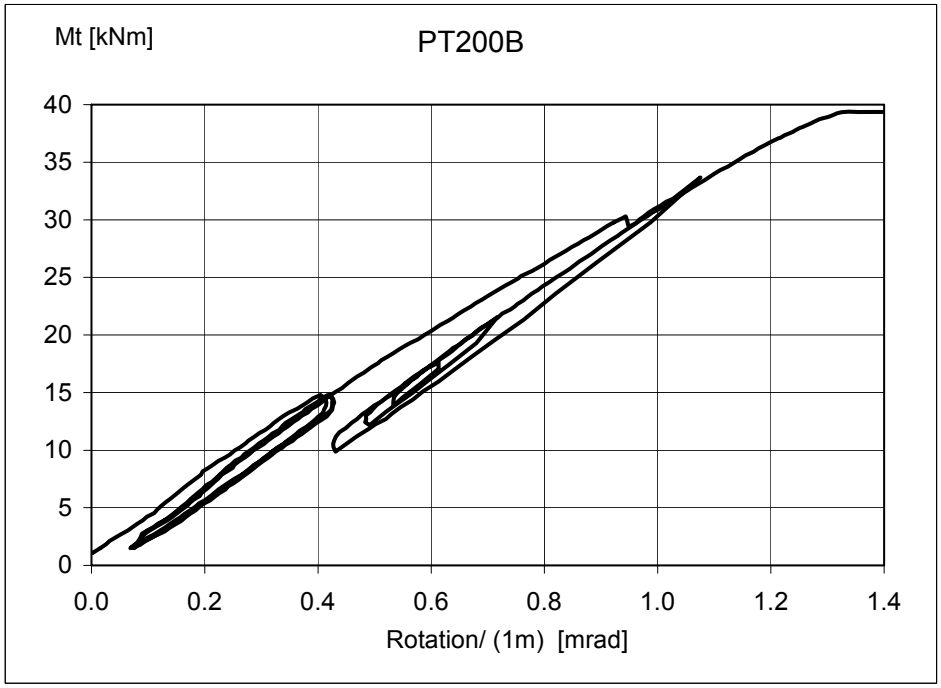

Fig. 13. PT200B. Interdependence of torque and relative angle of twist until cracking.

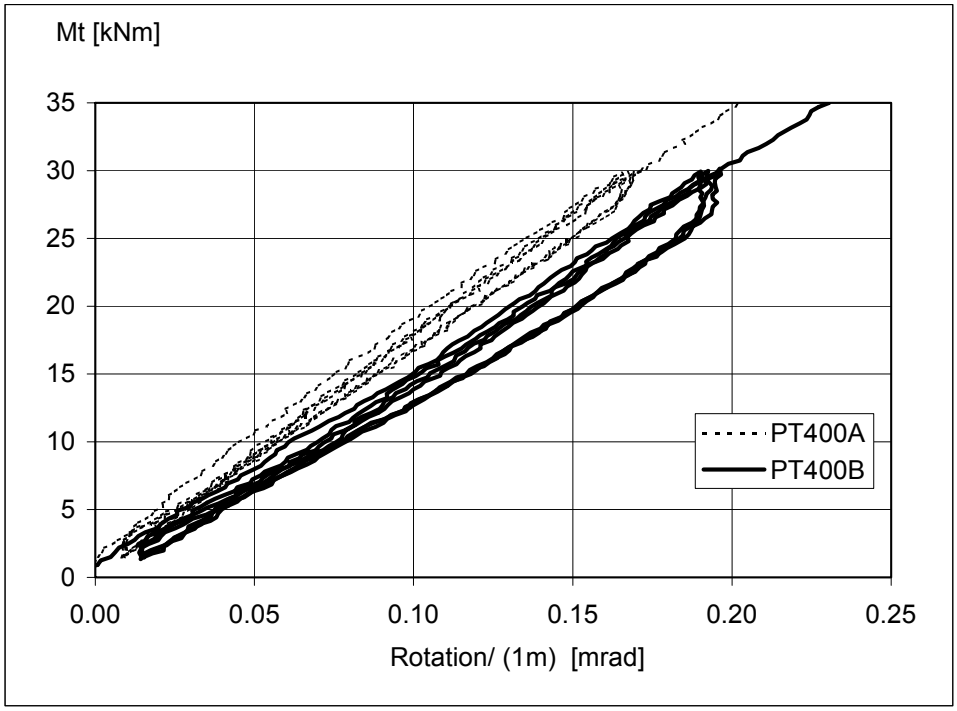

Fig. 14. PT400A and PT400B. Interdependence of torque and relative angle of twist until cracking.

In Figs 15 and 17 the whole torque vs. rotation relationship is illustrated and in Figs 16 and 18 the initial part of these curves. The curves in Figs 15–18 indicate the difficulty involved even in a displacement controlled load test when the concrete cracks. The event is too rapid to be recorded properly.

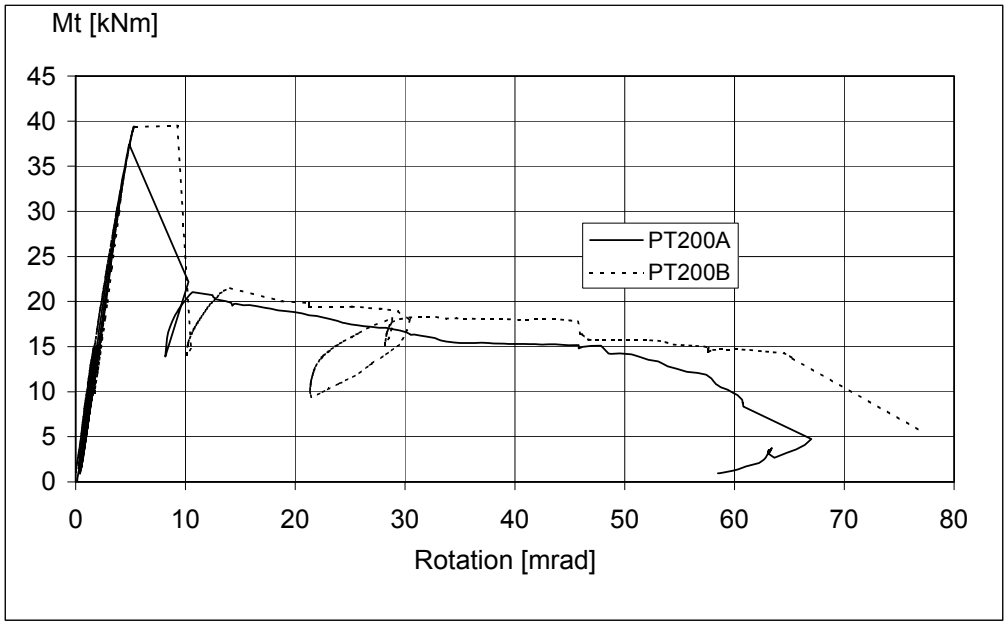

Fig. 15. Interdependence of torque and angle of twist for 200 mm slabs.

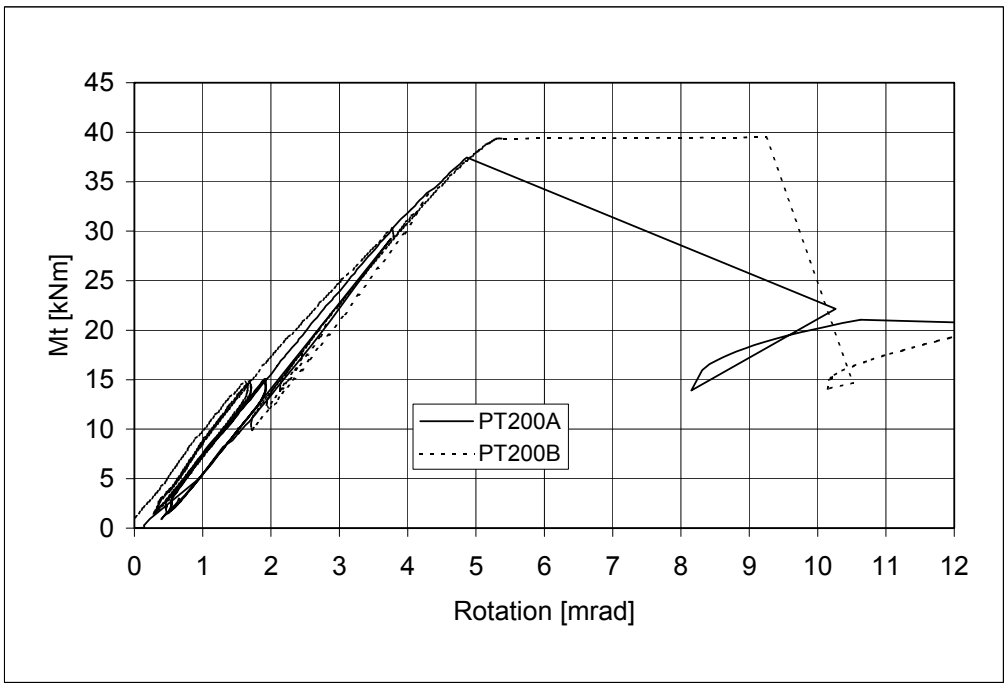

Fig. 16. Initial part of curves shown in previous figure.

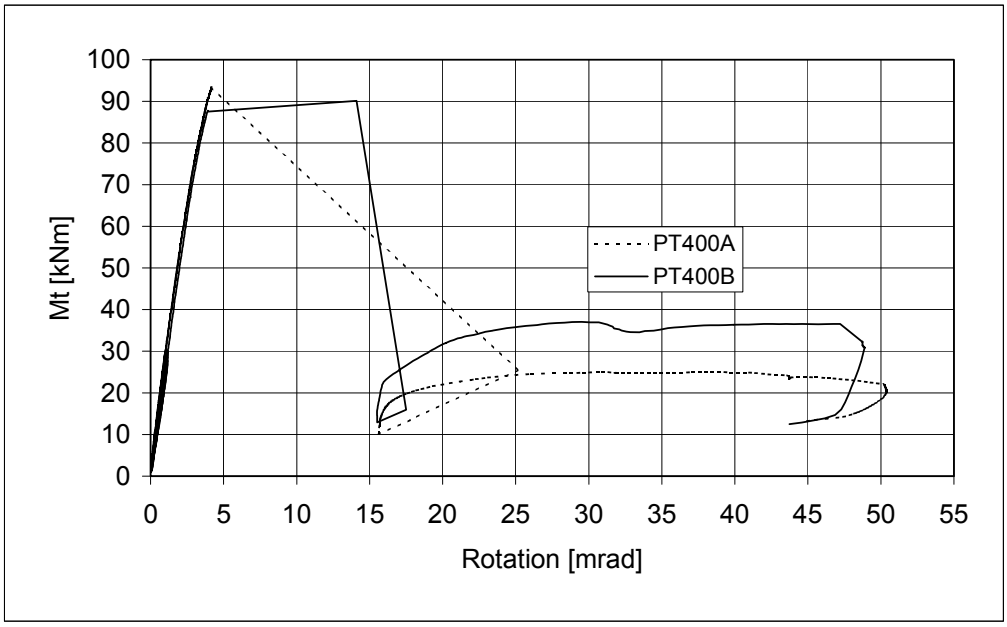

Fig. 17. Interdependence of torque and angle of twist for 400 mm slabs.

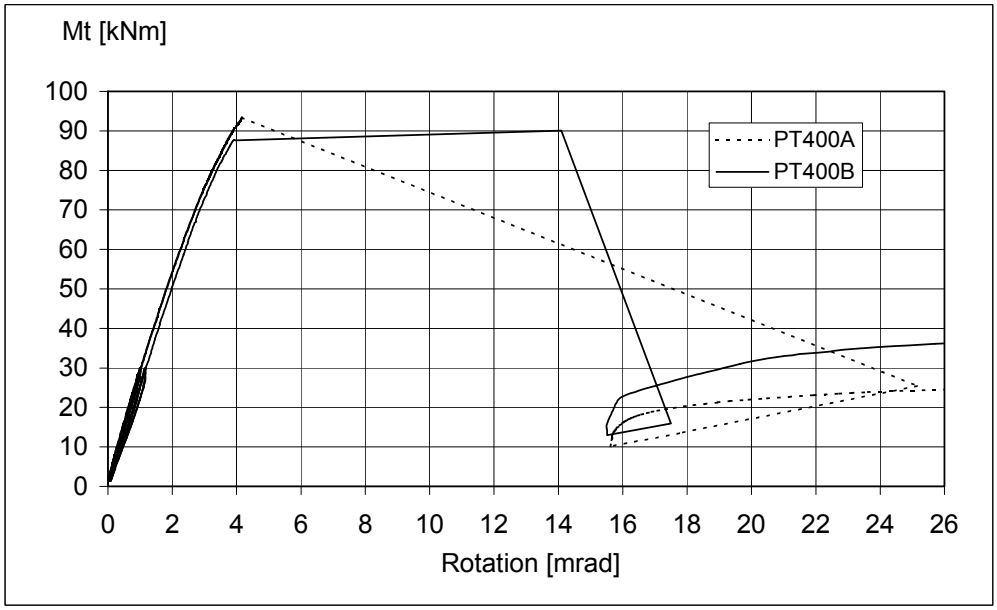

Fig. 18. Initial part of curves shown in previous figure.

In Fig. 19 the relative angle of twist is illustrated for all test specimens in the uncracked state. The slope of the curves gives the torsional stiffness of the slab unit.

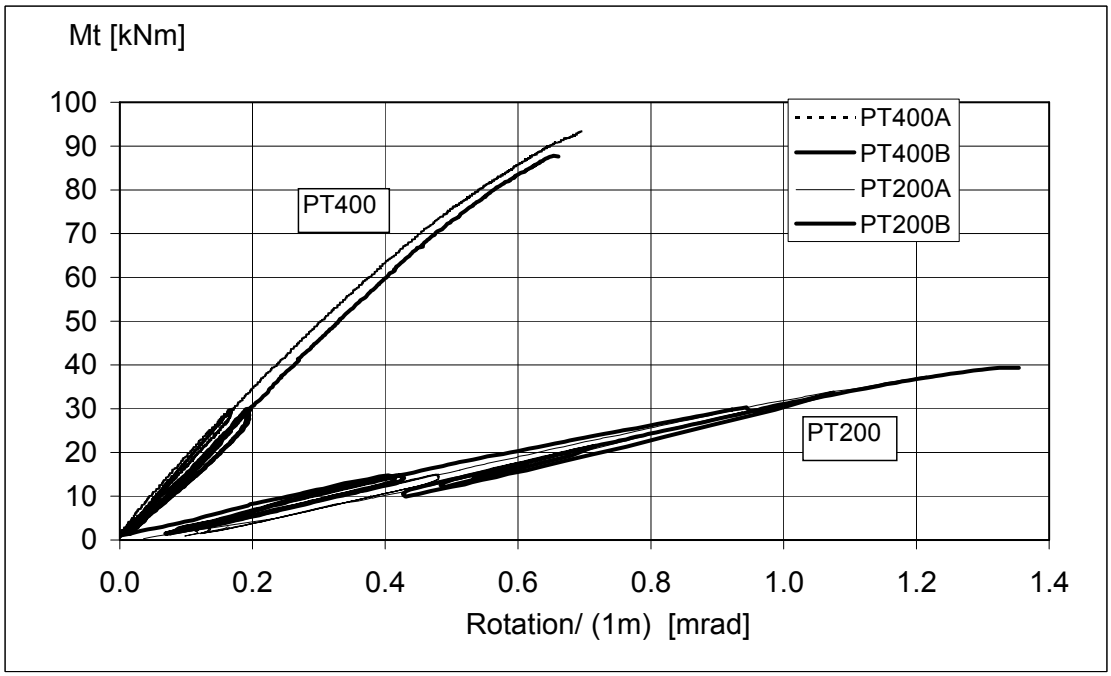

Fig. 19. Comparison of torsional stiffness of 200 and 400 mm slab units.

4.2 Data about concrete

The strength of the concrete was measured from drilled cores which were still wet due to the drilling and sawing when tested. For all slab units the measured strength was typical of normal production.

Table 2. Strength and density of 50 mm cores drilled from slab unit PT200A and tested on 13th of June 2002.

Specimen	Strength MPa	Density kg/m^3
PT21	66.5	2450
PT22	66.0	2490
PT23	67.0	2460
PT24	69.0	2450
PT25	59.5	2460
PT26	64.5	2440
Mean x	65.4	2458
Standard deviation s	3.2	17
Characteristic strength $f_{ck,C50} = x - 1.65s$	60.1	

Table 3. Strength and density of 50 mm cores drilled from slab unit PT200B and tested on 19th of June 2002.

Specimen	Strength MPa	Density kg/m^3
P27	62.0	2510
P28	73.0	2510
P29	66.0	2520
P30	69.0	2480
P31	62.5	2490
P32	74.5	2510
Mean x	67.8	2500
Standard deviation s	5.3	15
Characteristic strength $f_{ck,C50} = x - 1.65s$	59.2	

Table 4. Strength and density of 50 mm cores drilled from slab unit PT400A and tested on 19th of June 2002.

Specimen	Strength MPa	Density kg/m^3
P41	70.5	2490
P42	61.5	2490
P43	70.0	2510
P44	67.0	2500
P45	67.5	2510
P46	68.5	2500
Mean x	67.5	2492
Standard deviation s	3.2	26
Characteristic strength $f_{ck,C50} = x - 1.65s$	62.2	

In Table 5, data of the concrete mix, given by the manufacturer of the slabs, are given.

Table 5. Data about concrete mix.

Slab	P20	P40
Concrete	K60	K60
Cement	CEM I 52,5R	CEM I 52,5R
Number of aggregates	3	4
Maximum aggregate size	# 12 mm	# 16 mm
Water content	130 l/m^3	145 l/m^3

5. Analysis of results

It is assumed that the strength measured from 50 mm drilled cores gives directly the cubic strength measured from 150 mm cubes and that the cylinder strength is equal to 85% of the cubic strength. In this way, the lower characteristic cylinder strength $f_{ck,C150}$ (150 x 300 cylinders) given in Table 6 is obtained. From this, the mean tensile strength

$$f_{ctm} = 0.30 f_{ck,C150}^{2/3} \tag{2}$$

and the lower characteristic tensile strength

$$f_{ctk} = 0.70 f_{ctm} \tag{3}$$

are obtained according to Eurocode 2 [2] or CEB–FIP Model Code 1990 [1]. The elasticity modulus of concrete is calculated according to Model Code [1] from

$$E_c = 0.85 \cdot (21.5GPa) \cdot \left(\frac{f_{ck} + 8MPa}{10MPa} \right)^{1/3} \tag{4}$$

where the factor 0.85 takes into account the difference between initial and effective elasticity modulus. For the strands, elasticity modulus E_p = 195 GPa is used.

Table 6. Strength measured from 50 mm cores $f_{c,C50}$, corresponding cylinder strength $f_{c,C150}$, mean tensile strength f_{ctm}, characteristic tensile strength f_{ctk} and elasticity modulus E_c.

	$f_{c,C50}$ MPa	$f_{c,C150}$ MPa	f_{ctm} MPa	f_{ctk} MPa	E_c GPa
PT200A	60.1	51.1	4.15	2.91	33.0
PT200B	59.2	50.3	4.11	2.88	32.9
PT400A	62.2	52.9	4.25	2.97	33.4
PT400B	62.2	52.9	4.25	2.97	33.4

The interdependence of the torque M_t and relative angle of twist Θ is given by

$$M_t = GI_t\Theta \tag{5}$$

where $G = 0.5E/(1+\nu)$ and I_t denote the shear modulus and torsion modulus, respectively, and $\nu = 0.15$ denotes Poisson's ratio. Θ is defined by

$$\Theta = \frac{d\phi}{dx} \tag{6}$$

where ϕ denotes the angle of twist and x is the coordinate measured along the axis of the twisted member. In the present tests

$$\Theta = \frac{\phi}{L} \tag{7}$$

can be written where L is the span of the slab unit and ϕ the rotation of the active end with respect to the passive end. For a hollow core cross-section, replacing the cross-section with a tubular one as shown in Fig. 20, I_t can be calculated from

$$I_t = \frac{2t_1t_2(h-t_2)^2(b-t_1)^2}{bt_1 + ht_2 - t_1^2 - t_2^2} \tag{8}$$

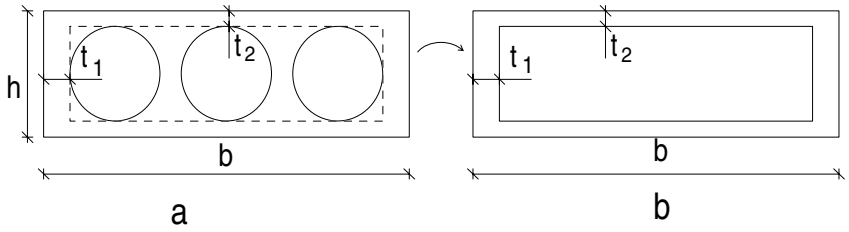

Fig. 20. Transforming a hollow core cross-section (a) into a tubular cross-section (b).

The maximum shear stress $\tau_{t,max}$ due to M_t can be evaluated using

$$\tau_{t,\max} = \frac{M_t}{W_t} \tag{9}$$

where the section modulus in torsion for the web can be calculated from

$$W_{t1} = 2t_1(h-t_2)(b-t_1) \tag{10}$$

and that for the top flange from

$$W_{t2} = 2t_2(h-t_2)(b-t_1) \tag{11}$$

Table 7 gives both the geometry of the tubular slab cross-section without inner webs and the resulting geometric moduli. The width and depth of the cross-section are

nominal values. The thickness of flanges and outer webs are means of measured values. To simplify the calculations, the thickness of the top flange is also used for the bottom flange. The error due to this is small because the measured thicknesses were close to each other.

Table 7. Geometry and torsional characteristics of tubular cross-section. Width b and depth h of whole section, thickness of web t_1, bottom flange $t_{2,bot}$ and top flange $t_{2,top}$, torsion modulus I_t as well as section moduli in torsion W_{t1} (web) and W_{t2} (top flange).

	b mm	h mm	t_1 mm	$t_{2,bot}$ mm	$t_{2,top}$ mm	I_t mm^4	W_{t1} mm^3	W_{t2} mm^3
PT200A	1160	200	27.5	23.1	23.8	1.48E+09	1.10E+07	9.50E+06
PT200B	1160	200	28.5	24.0	23.9	1.48E+09	1.14E+07	9.52E+06
PT400A	1160	400	51.3	38.0	39.0	9.03E+09	4.11E+07	3.12E+07
PT400B	1160	400	54.0	39.4	41.0	9.38E+09	4.29E+07	3.26E+07

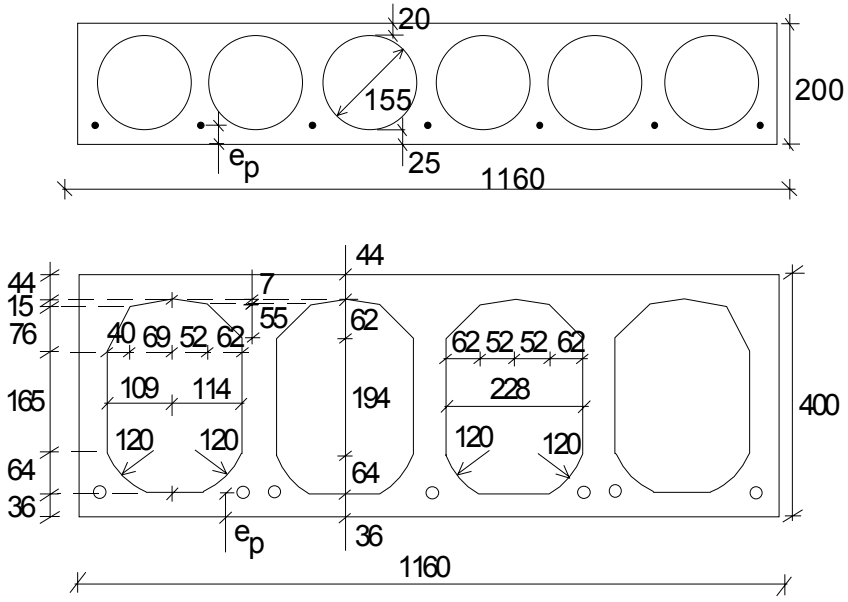

Figure 21. Geometry used for stress analysis in longitudinal and vertical direction.

Table 8 gives the cross-sectional characteristics of the hollow core slabs specified in Fig. 21. The measured average web width b_w and the first moment of area S are also given, even though they are not needed when analysing the normal stresses in the top flange.

Using the data from Tables 7 and 8 and assuming the loss of prestress equal to 50 MPa, the predicted results given in Table 9 are obtained. The torsional stiffness is calculated using only the monotonous[1] loading stage starting after the last unloading in the cyclic stage and ending at the last step before cracking. Cracking of the top flange above the support is the critical failure mode. The results given in Table 10 are calculated assuming the loss of prestress equal to 100 MPa. Based on Tables 9 and 10 it can be concluded that the results are not sensitive to the exact estimation of the losses of prestress.

Table 8. Distance from centroid of strands to the bottom fibre e_p, distance from centroidal axis to bottom fibre e, sum of web widths b_w, cross-sectional area A, second moment of area I and first moment of area S.

	e_p mm	e mm	b_w mm	A mm^2	I mm^4	S mm^3
PT200A	38.1	96.1	223	122000	$6.13 \cdot 10^8$	$4.02 \cdot 10^{6}$ *)
PT200B	38.5	96.1	227	122000	$6.13 \cdot 10^8$	$4.02 \cdot 10^{6}$ *)
PT400A	36.6	206.3	276	210800	$4.43 \cdot 10^9$	$1.41 \cdot 10^7$
PT400B	34.6	206.3	285	210800	$4.43 \cdot 10^9$	$1.41 \cdot 10^7$

*) *First moment of area above the thinnest part of the web*

Table 9. Comparison of predicted and observed torsional stiffness GI_t and resistance against torque M_t, when loss of prestress is = 50 MPa. ϕ_{obs} is the last observed angle of twist between supports before cracking.

	$M_{t,obs}$ kNm	ϕ_{obs} mrad	$M_{t,pre}$ 1) kNm	$M_{t,pre}$ 2) kNm	$GI_{t,obs}$ MNm^2	$\frac{GI_{t,pre}}{GI_{t,obs}}$	$\frac{M_{t,pre}}{M_{t,obs}}$ 1)	$\frac{M_{t,pre}}{M_{t,obs}}$ 2)
PT200A	37.45	4.86	34.9	22.9	32.91	0.64	0.93	0.61
PT200B	39.38	5.35	34.8	22.9	30.02	0.71	0.88	0.58
PT400A	92.96	4.17	103.6	61.74	133.1	0.98	1.11	0.66
PT400B	87.38	3.92	106.9	63.05	134.7	1.01	1.22	0.72

1) *Calculated using mean tensile strength f_{ctm}*
2) *Calculated using lower characteristic tensile strength f_{ctk}*

[1] In test PT200B this stage was not monotonous

Table 10. *Comparison of predicted and observed resistance against torque M_t, when loss of prestress is = 100 MPa. The symbols have the same meaning as in Table 9.*

	$M_{t,pre}$ [1)] kNm	$M_{t,pre}$ [2)] kNm	$\frac{M_{t,pre}}{M_{t,obs}}$ [1)]	$\frac{M_{t,pre}}{M_{t,obs}}$ [2)]
PT200A	34.9	22.9	0,94	0,62
PT200B	34.8	22.9	0,89	0,59
PT400A	103.6	61.74	1,13	0,68
PT400B	106.9	63.05	1,24	0,74

[1)] *Calculated using mean tensile strength f_{ctm}*
[2)] *Calculated using lower characteristic tensile strength f_{ctk}*

Comparison with the observed values shows that the torsional stiffness of the 400 mm slabs is accurately predicted by the simple calculation method, but that of the 200 mm slabs is underestimated by 30%. This difference cannot be eliminated by changing the value of elasticity modulus in calculations. Numerical analysis is needed to clarify the reasons for such a big difference.

The resistance, calculated using the mean tensile strength, is higher than the observed one for 400 mm slabs, but lower than the observed resistance for the 200 mm slabs. Using the characteristic tensile strength instead of the mean tensile strength reduces the predicted values so much that the ratio of predicted to observed resistance becomes roughly 70% and 60% for 400 mm and 200 mm slabs, respectively.

6. Discussion

When the slab units are cut by sawing, the concrete has not reached its final strength. The mechanical actions of the high speed saw may locally cause longitudinal cracks of the type shown in Fig. 22. Such cracks, due to sawing or other reasons, may sometimes be very long. In the present slab units no visible, longitudinal cracks were observed in the top flange before the test but some local damage may have existed.

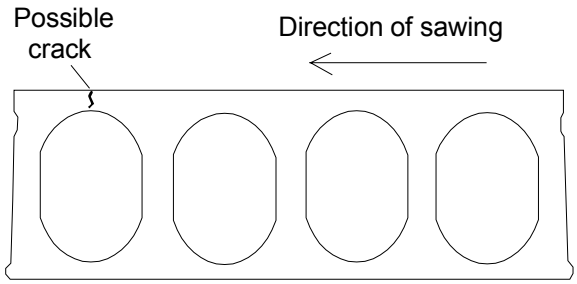

Fig. 22. Crack caused by sawing.

Thanks to the test arrangements, the tensile stresses in the concrete above each hollow core were almost uniformly distributed in the longitudinal direction. An increasing and uniformly distributed tensile stress tends to seek the weakest point of the concrete. For this reason the lower characteristic value of the tensile strength is a good starting point for calculation of torsional resistance and for comparison of calculated and observed resistance in the present tests. When this is done, see the last column in Table 9, the results suggest that the lower characteristic value or an even more conservative value for the resistance can be obtained by applying elementary calculation methods.

One might expect, that a fairly conservative approximation for the torsional stiffness is obtained by omitting the inner parts of the slab cross-section and calculating the torsional stiffness as for a tubular cross-section with thickness equal to the minimum thickness of the top flange or minimum thickness of the outer webs. This is, indeed, the case for 200 mm slabs, for which the calculated stiffness was roughly 70% of the observed stiffnes. For 400 mm slabs the calculated and observed stiffness were equal. This is difficult to explain. Further numerical research is needed.

References

1. CEB-FIP Model Code 1990. Comité Euro-International du Béton. Thomas Telford, London 1993. ISBN: 0 7277 1696 4.

2. EN 1992-1-1. Eurocode 2: Design of concrete structures – Part 1: General rules and rules for buildings. 2004.

Appendix A: Photographs

The red numbers on the surface of the slabs refer to the actuator load. They tell the load at which the crack formed.

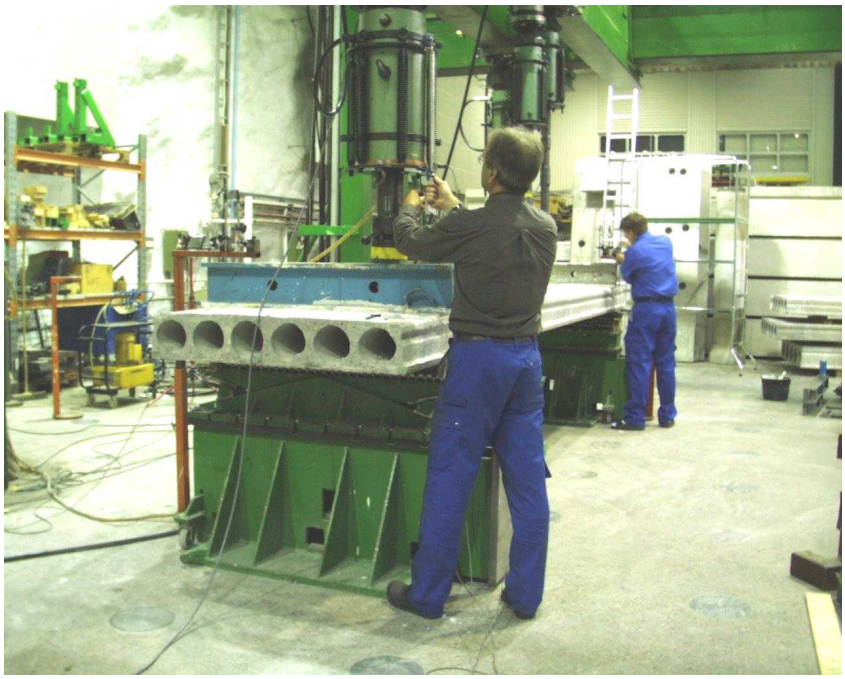

Fig. 1. PT200A. Completing test arrangements.

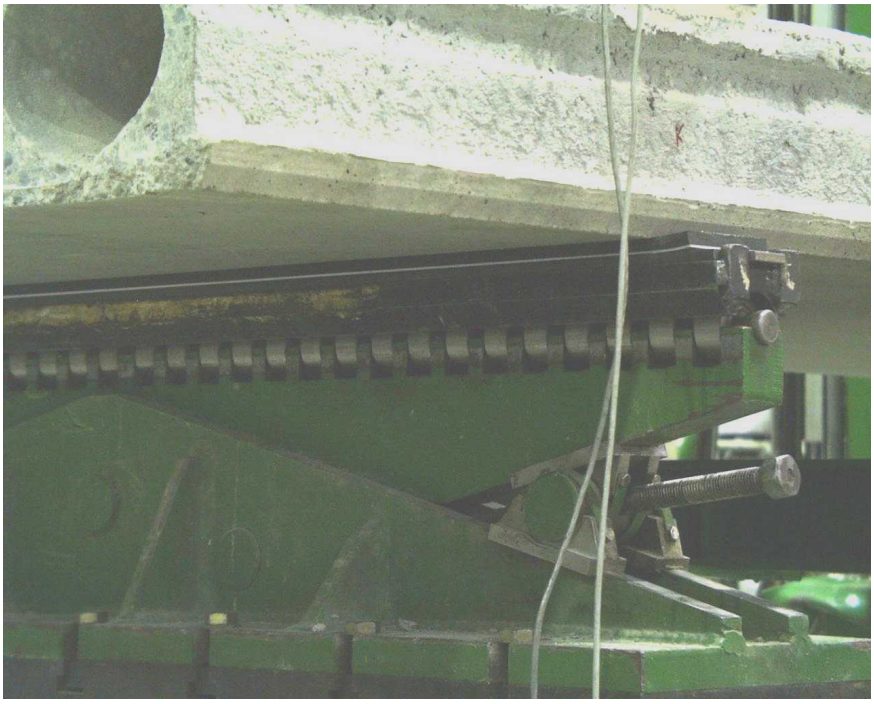

Fig. 2. PT200A. Detail of support at active end before the test. Rotation of active end prevented by an adjustable wedge on the right.

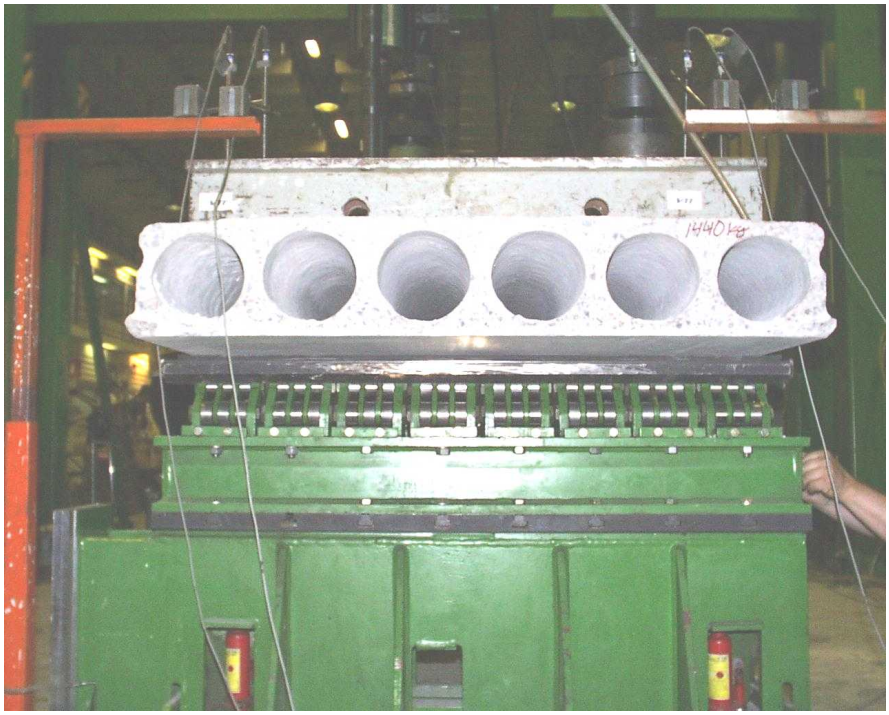

Fig. 3. PT200A. Support at passive end.

Fig. 4. PT200A. Support at passive end. Side view.

Fig. 5. PT200A. Side view on test arrangements. The two actuators in the middle were not used.

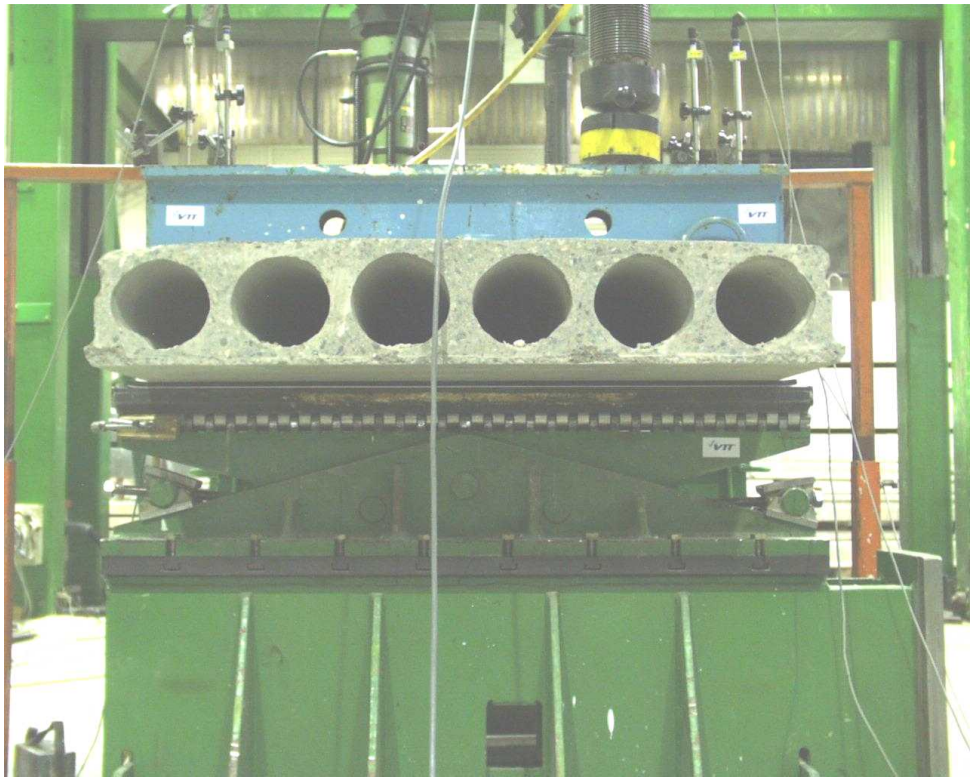

Fig. 6. PT200A. Active end. Rotation of the slab end allowed.

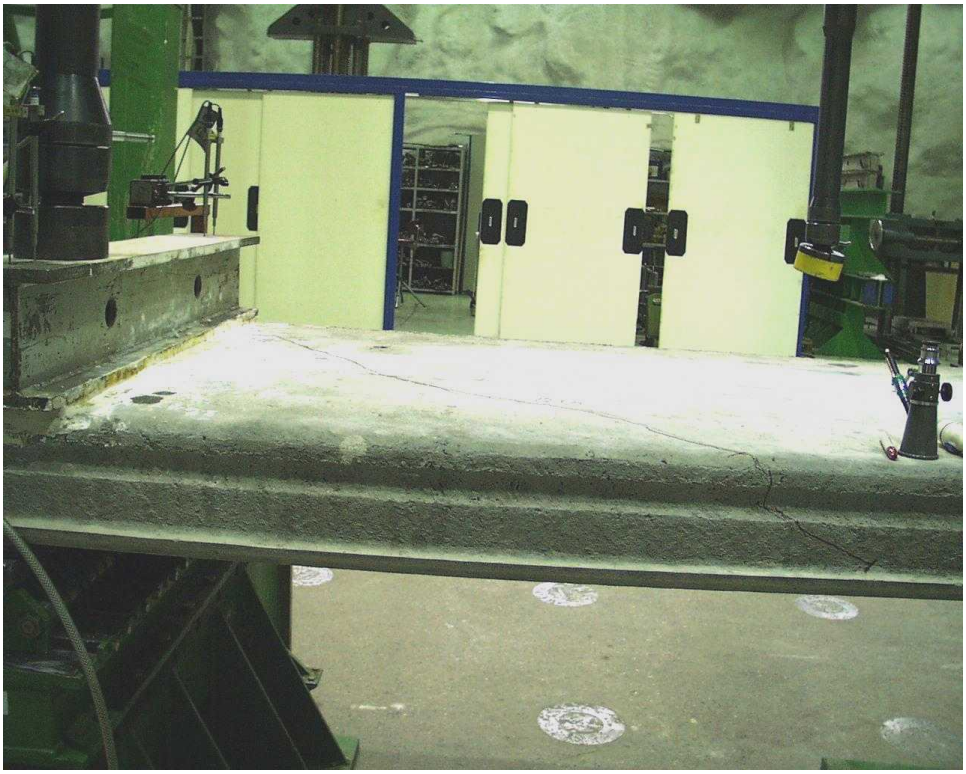

Fig. 7. PT200A. Passive end after first cracks had appeared.

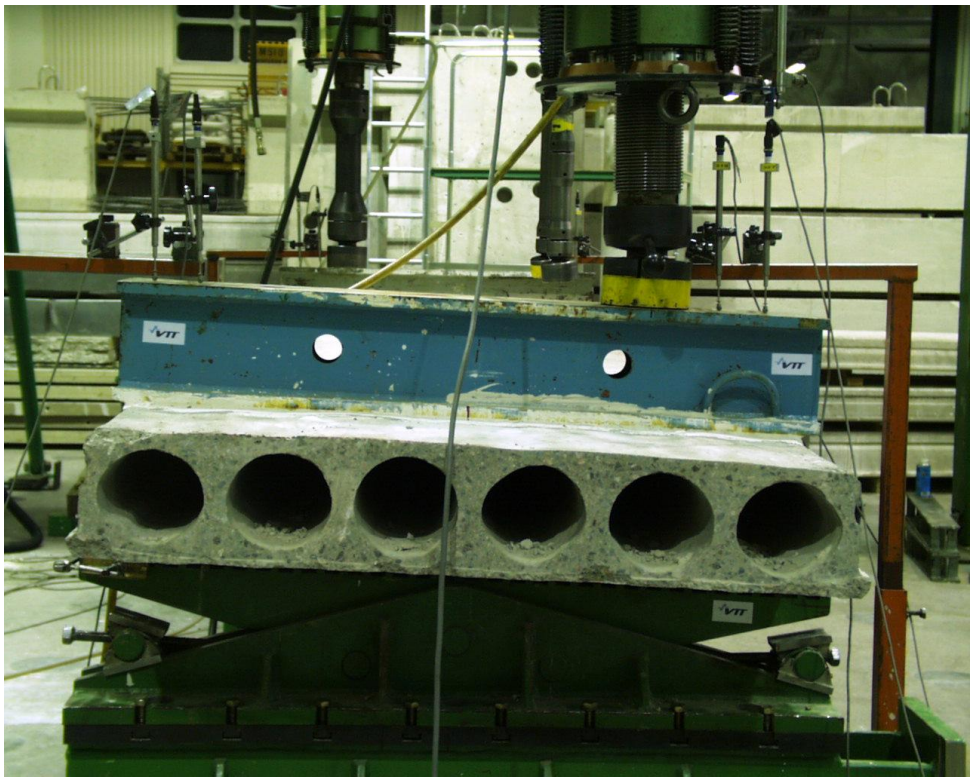

Fig. 8. PT200A. Active end before failure.

Fig. 9. PT200A. Detail of crack after failure.

Fig. 10. PT200A. Side view after failure.

Fig. 11. PT200A. Side view after failure.

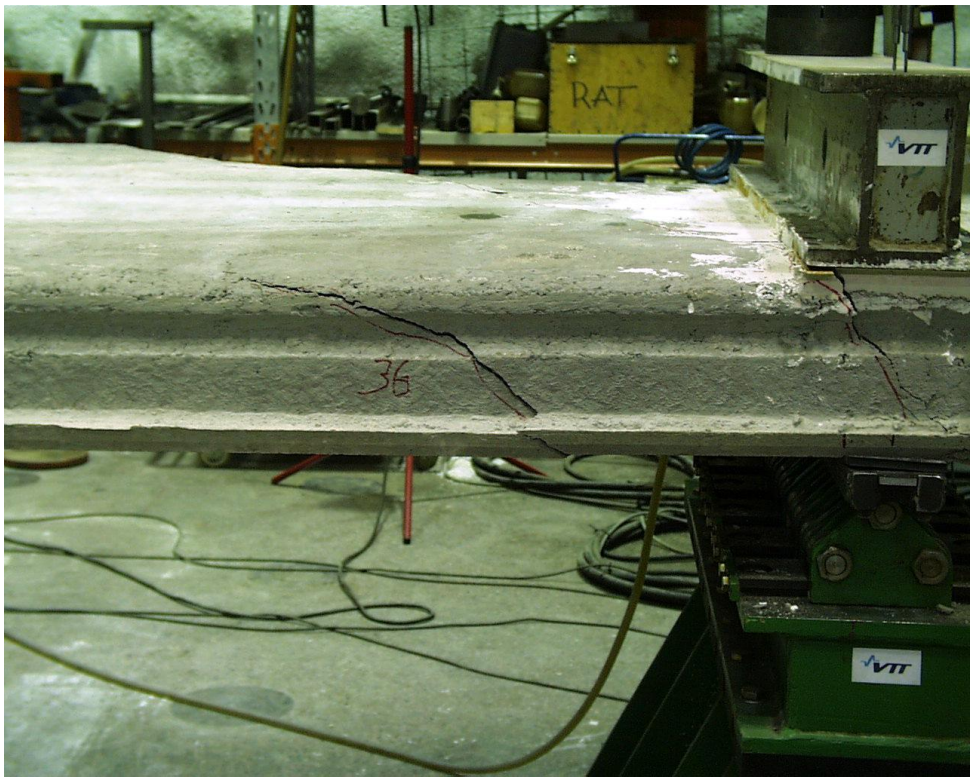

Fig. 12. PT200A. Secondary cracking of the edge opposite to the primary cracking. The red figures refer to the applied actuator load.

Fig. 13. PT200A. Cracks on the top of the slab after failure.

Fig. 14. PT200A. Cracking pattern at the cantilevered passive end after failure.

Fig. 15. PT200A. Cracking pattern after failure. The red figures refer to the applied actuator load.

Fig. 16. PT200A. Cracking pattern at the soffit of the slab after failure.

Fig. 17. PT200B. Cracking pattern at passive end.

Fig. 18. PT200B. Cracking of cantilevered passive end.

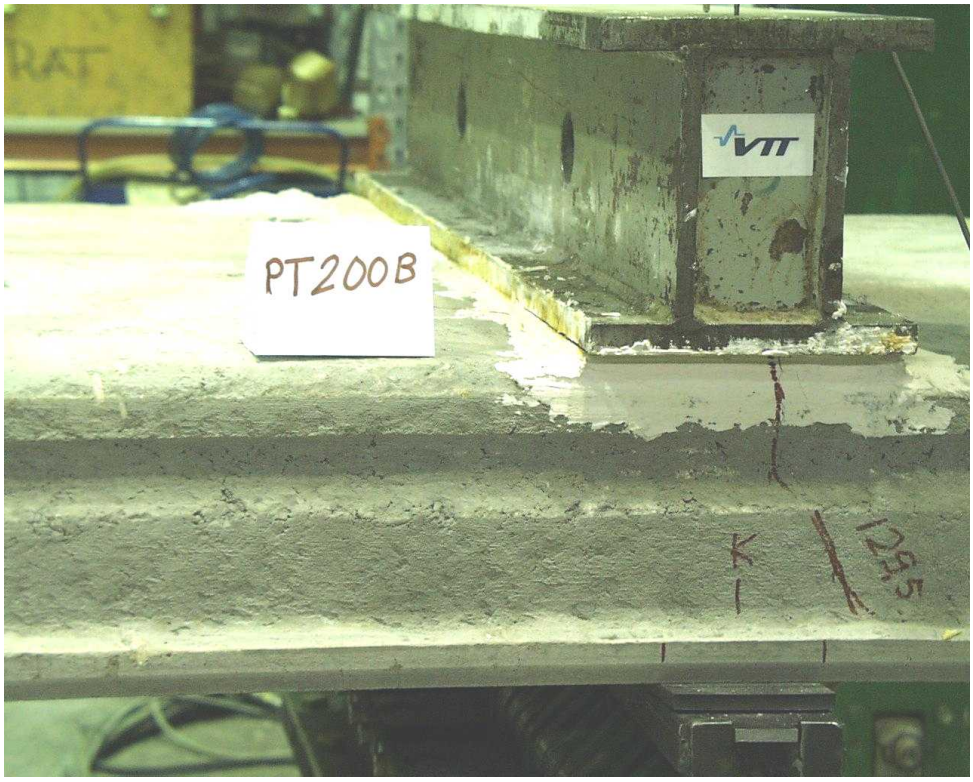

Fig. 19. PT200B. Cracking below the spreader beam at passive end.

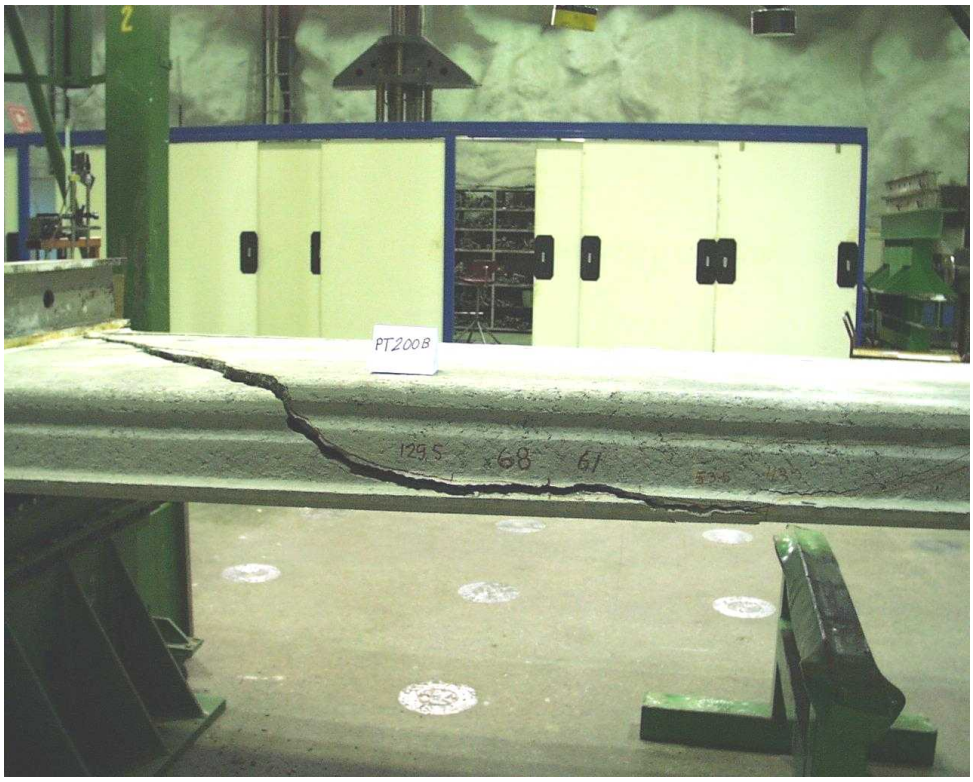

Fig. 20. PT200B. Cracking pattern after failure.

Fig. 21. PT200B. Cracking pattern after failure.

Fig. 22. PT200B. Cracking pattern after removal of loads and loading equipment.

Fig. 23. PT200B. Crackingpattern after removal of loads and loading equipment.

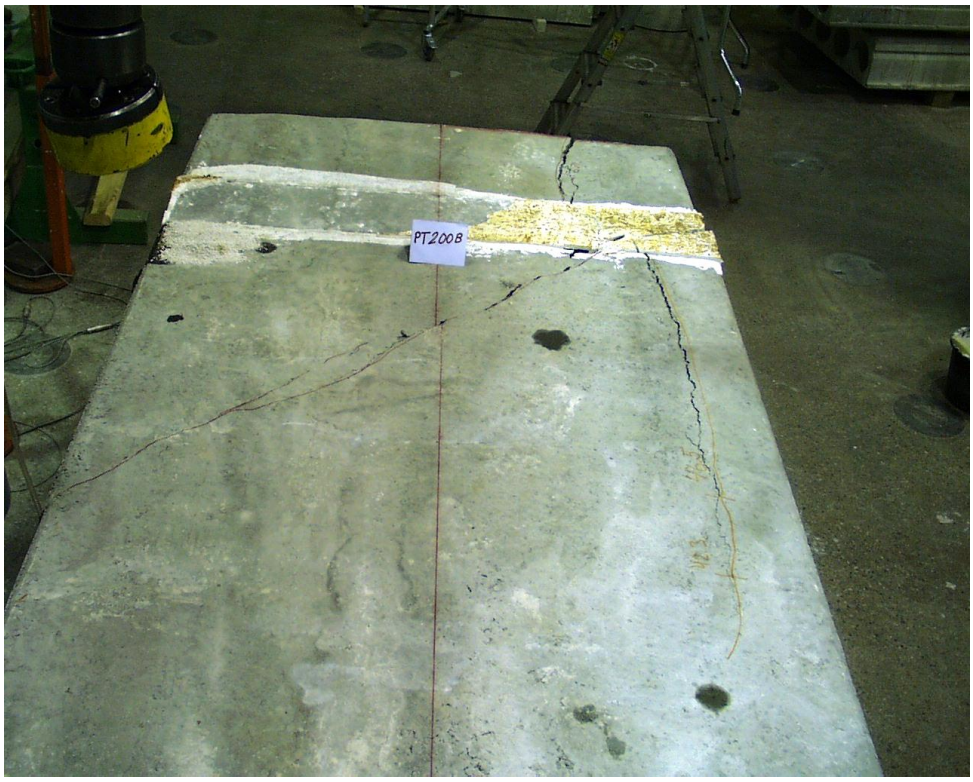

Fig. 24. PT200B. Cracks on the top surface after removal of loads and loading equipment.

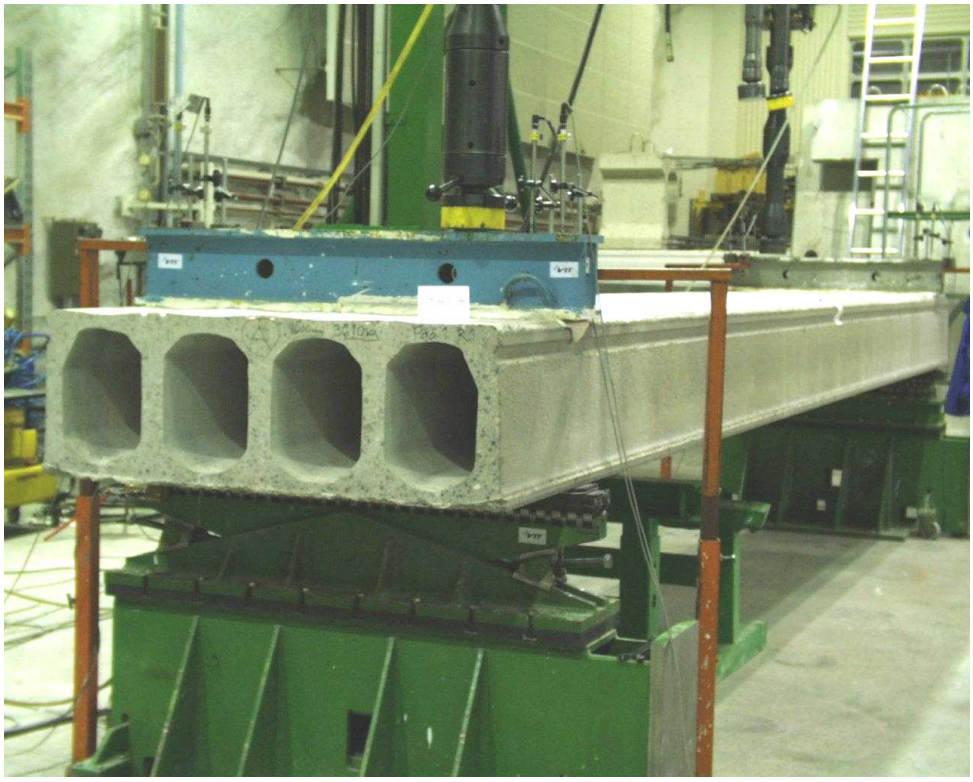

Fig. 25. PT400A. General view on the test layout.

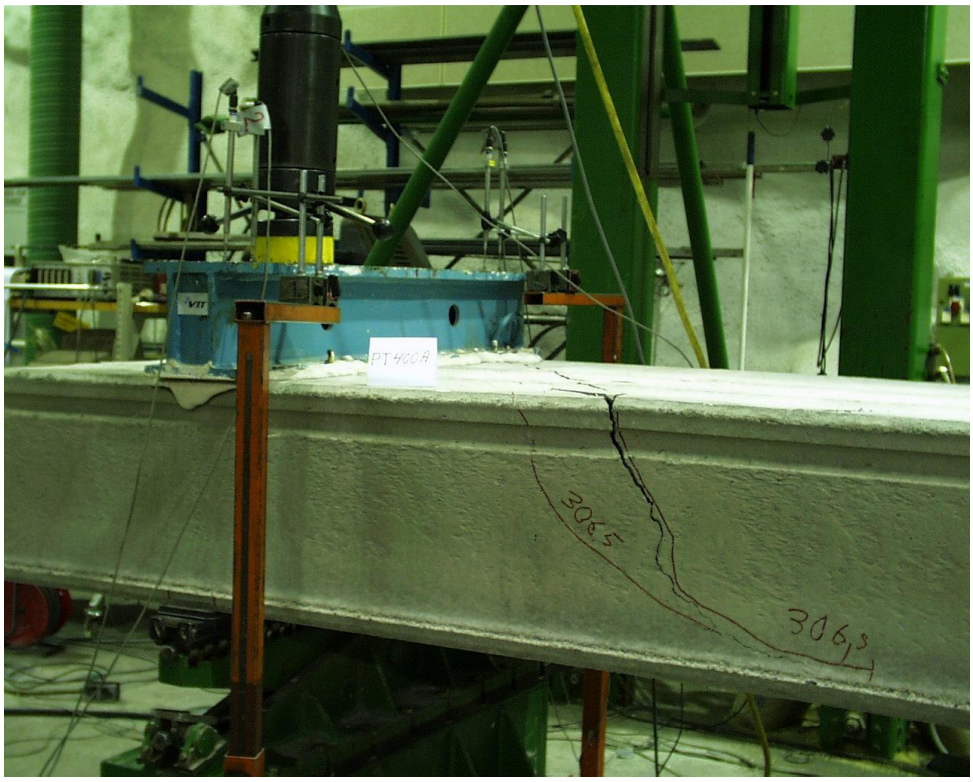

Fig. 26. PT400A. Cracking pattern at the active end.

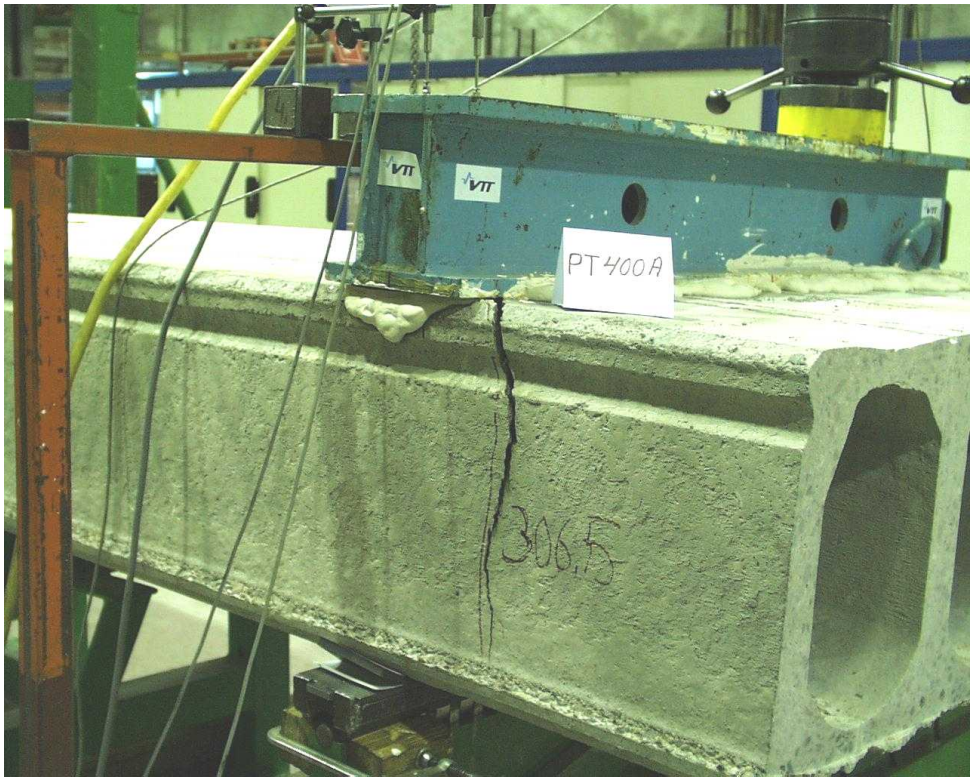

Fig. 27. PT400A. Vertical crack outside the spreader beam.

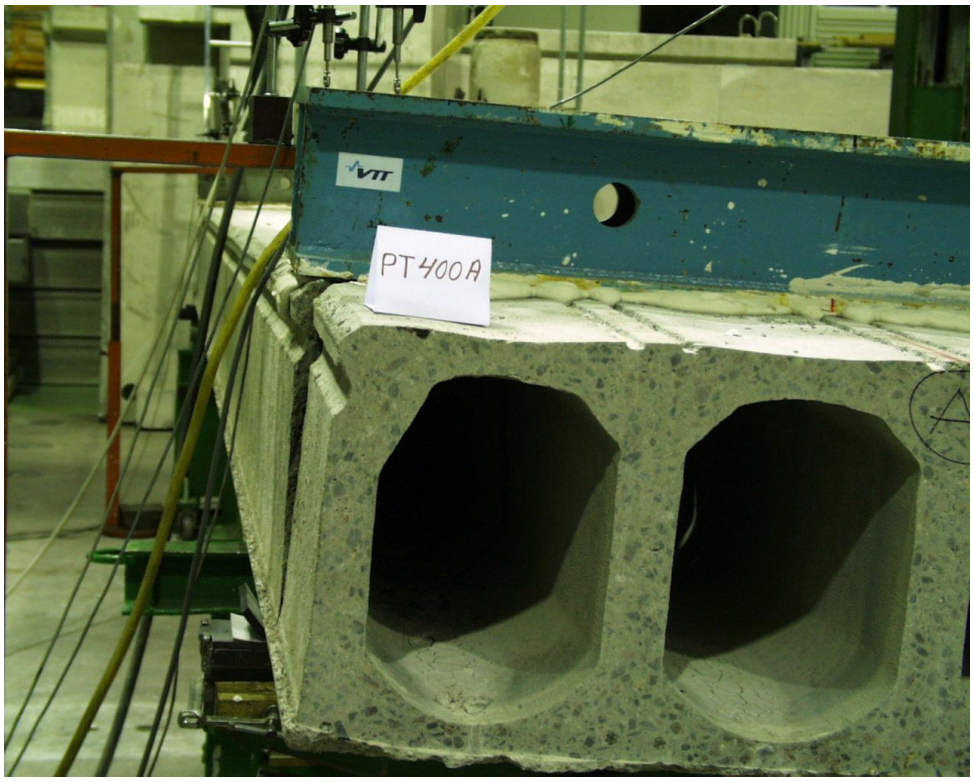

Fig. 28. PT400A. Active end after failure.

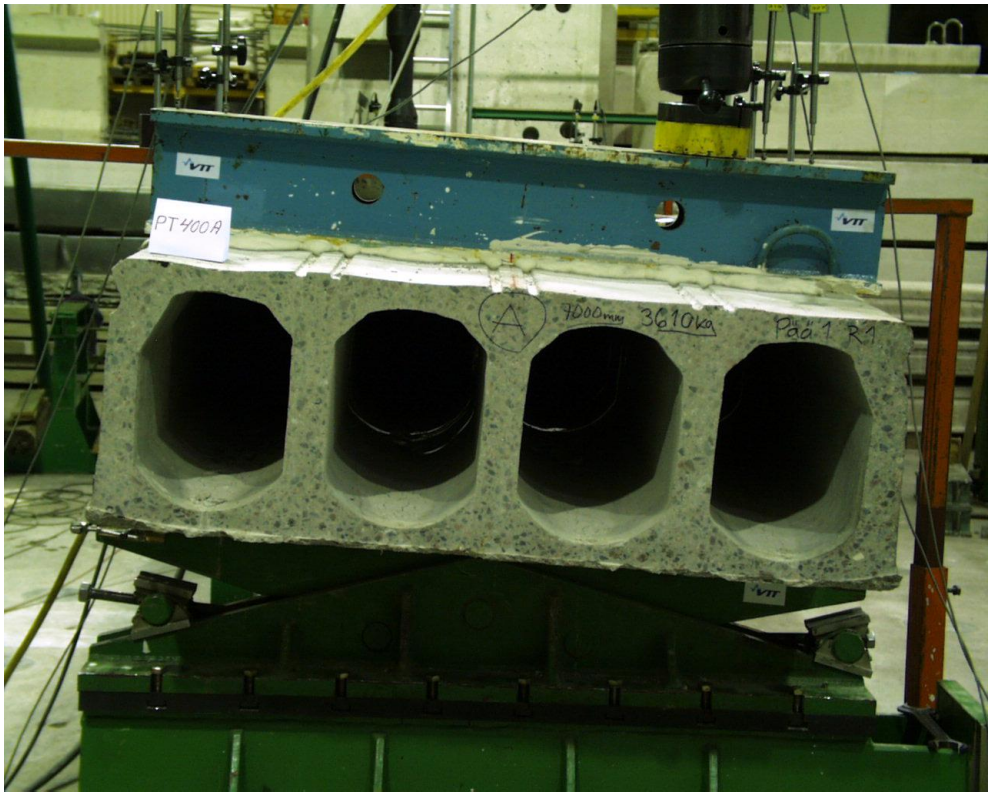

Fig. 29. PT400A. Rotation of active end after failure.

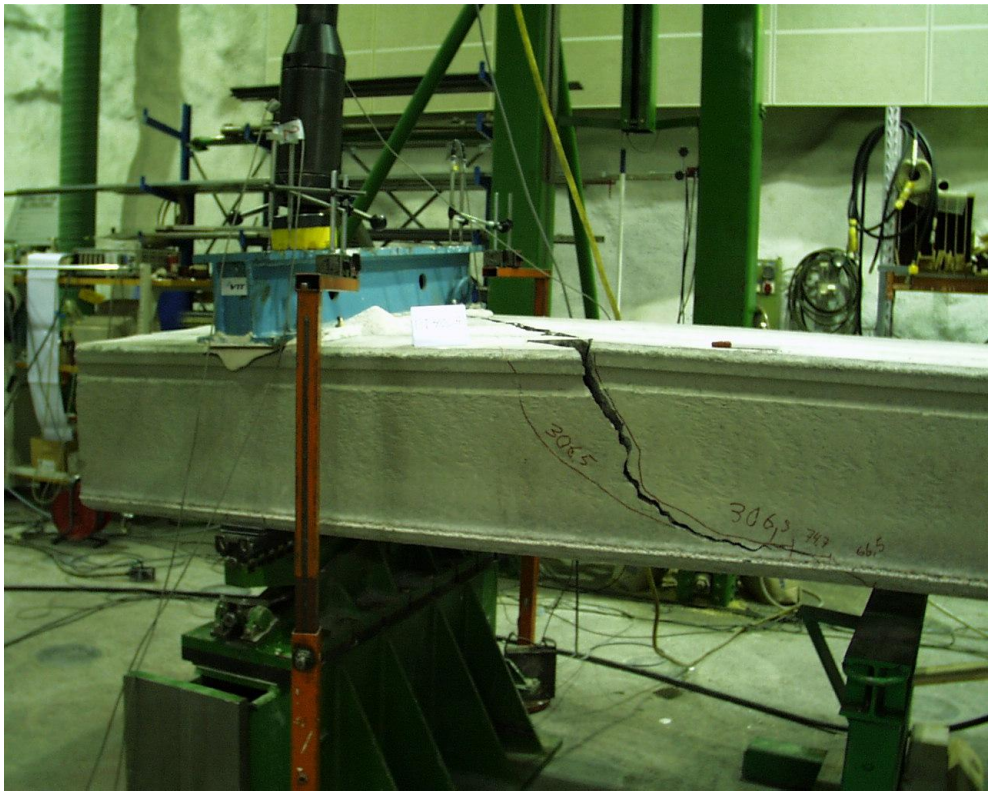

Fig. 30. PT400A. Cracking pattern after failure.

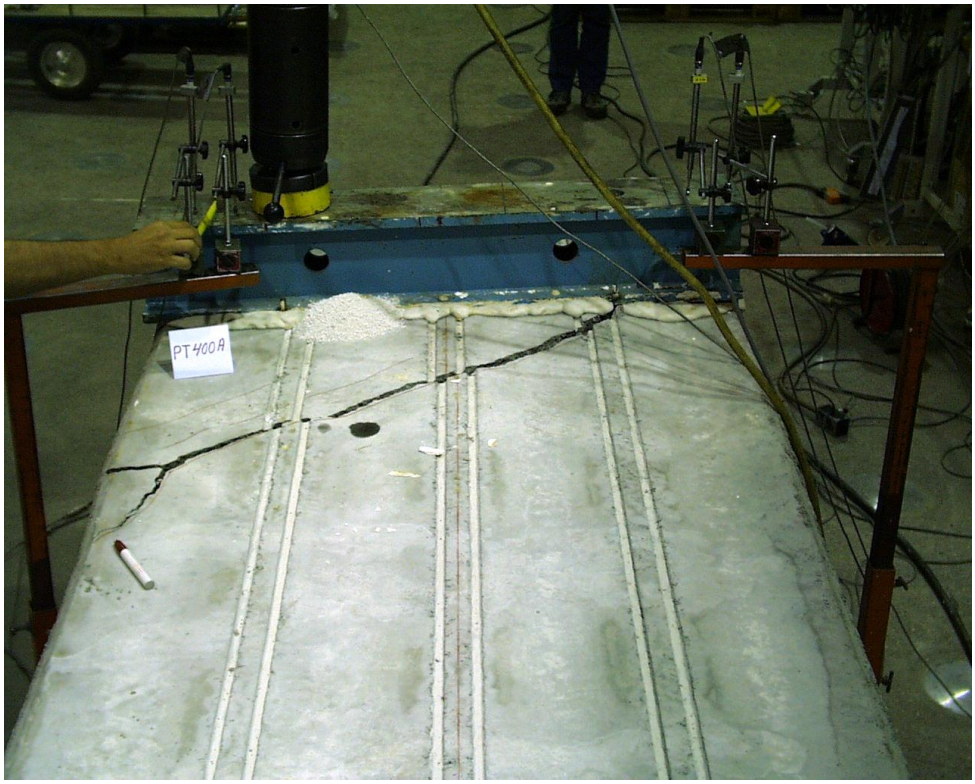

Fig. 31. PT400A. Cracking pattern on the top of the slab.

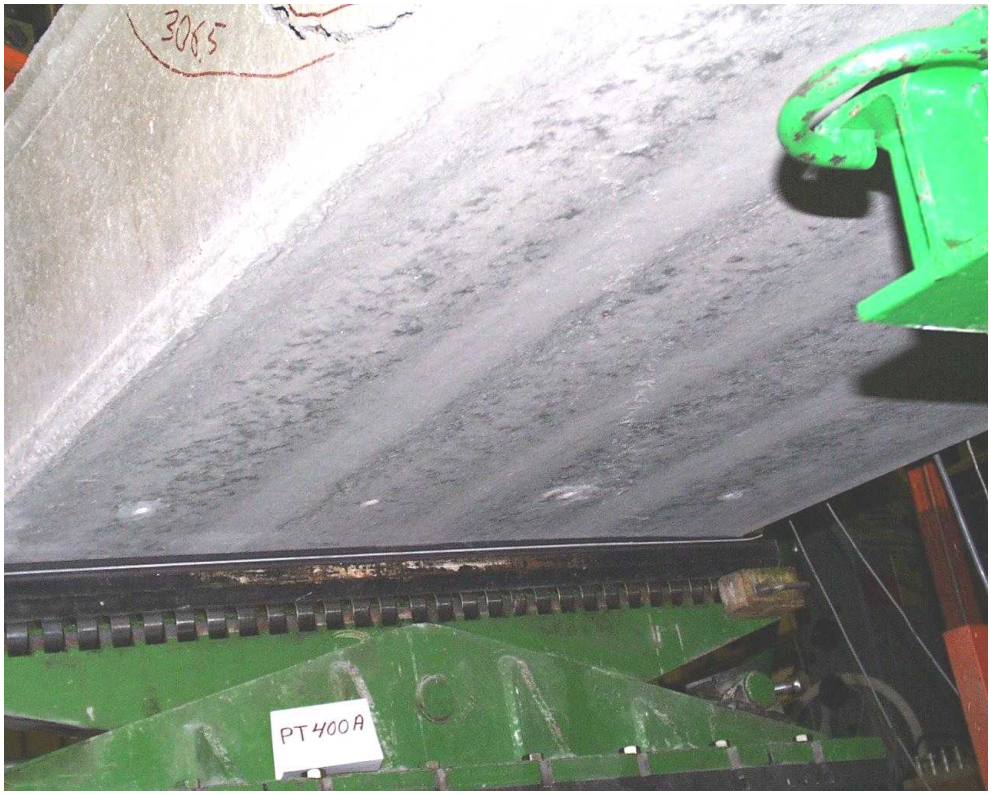

Fig. 32. PT400A. Cracking pattern at the soffit of the slab.

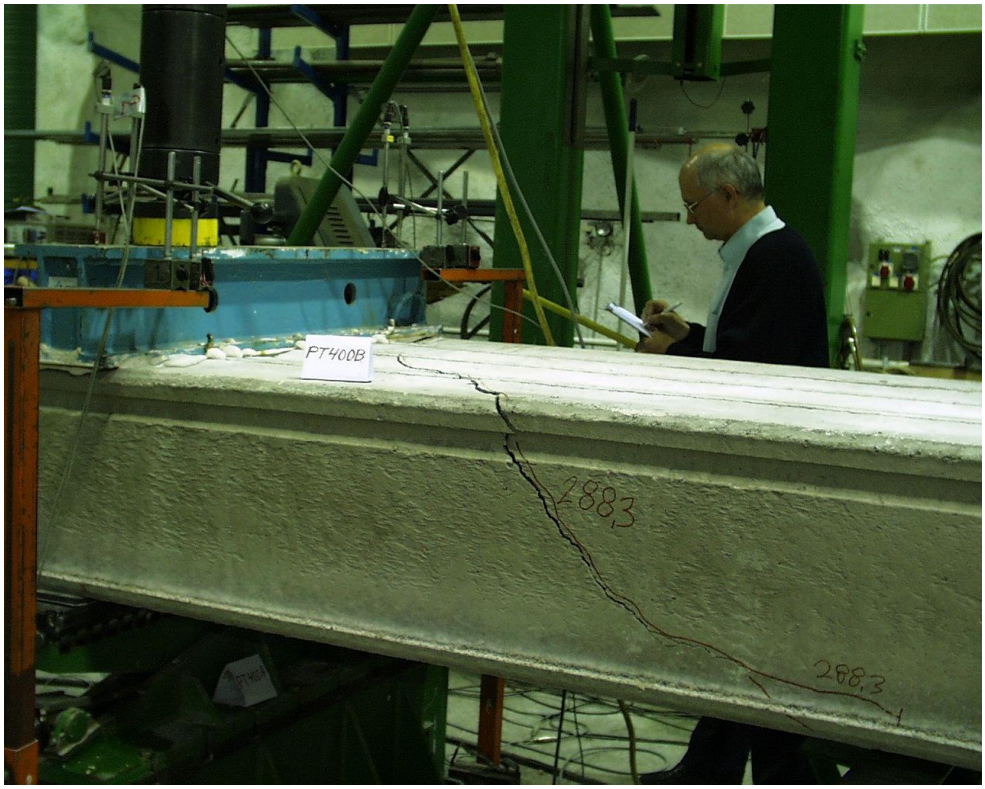

Fig. 33. PT400B. Cracking pattern at the active end.

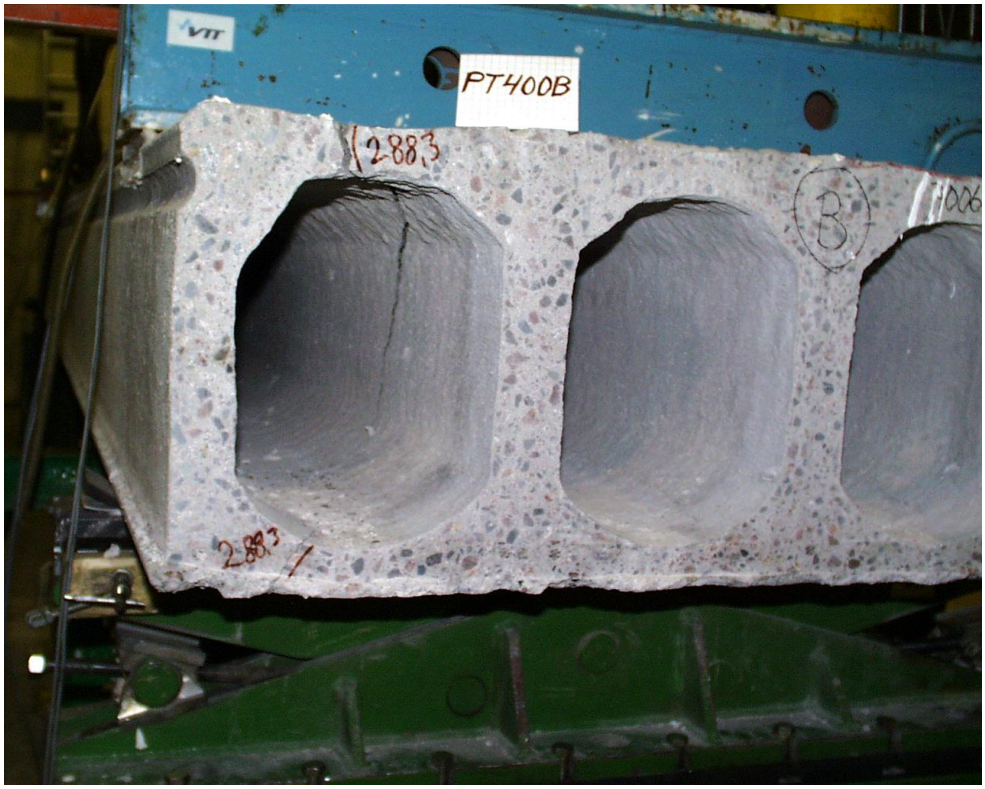

Fig. 34. PT400B. Cracking of the cantilevered end.

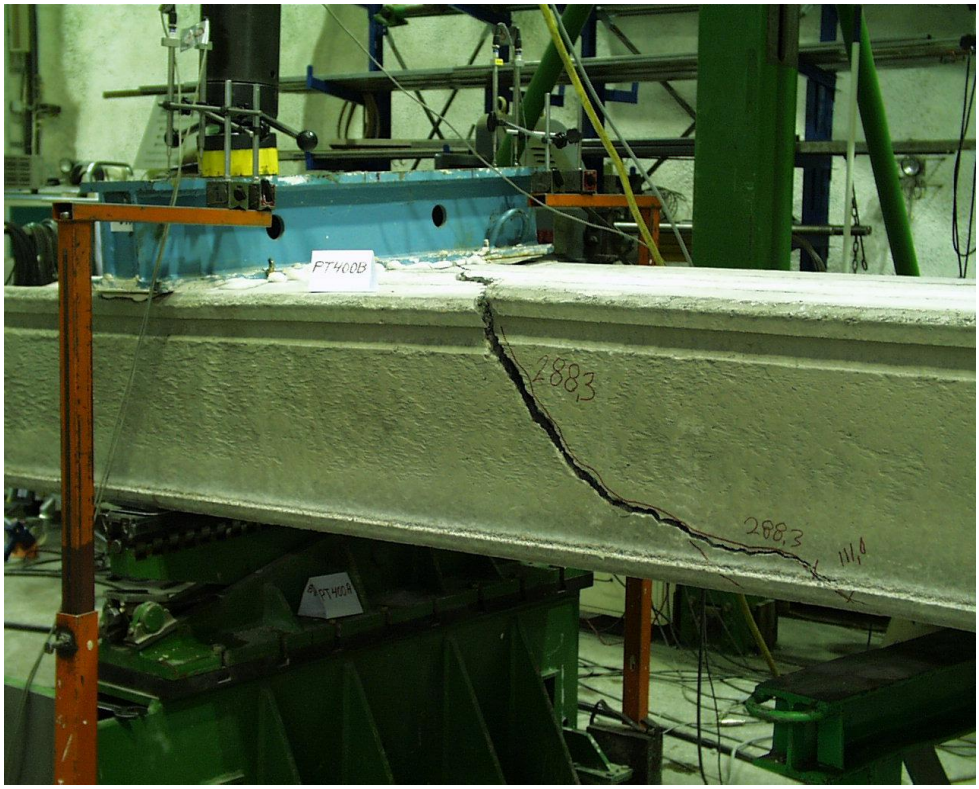

Fig. 35. PT400B. Cracking after failure.

Fig. 36. PT400B. Soffit of slab after failure.

Fig. 37. PT400B. Detail of soffit after failure

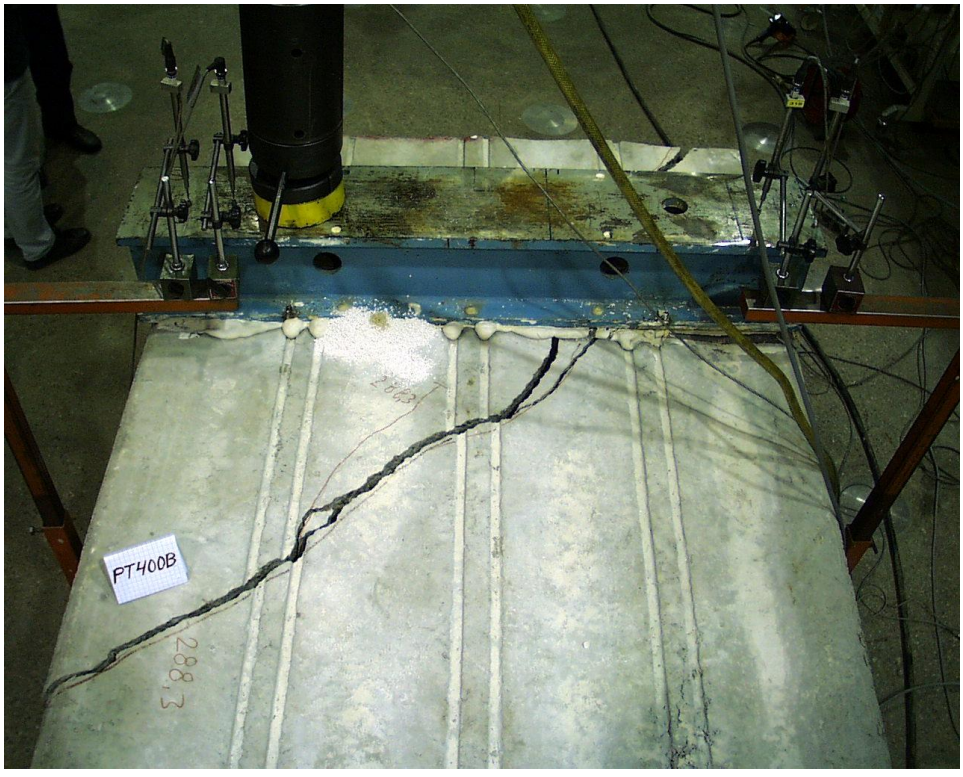

Fig. 38. PT400B. Top surface after failure.

Appendix B: Measured geometry of slabs

In the following figures *prestress* refers to the nominal prestress in the strands after pretensioning (initial prestress). The underlined values refer to initial slippage of the strands. The strands are made of seven non-indented (smooth) wires. The cross-sectional area of a strand is 93 mm^2 and nominal strength 1640 MPa / 1860 MPa (0.2% yield strength / ultimate strength). All data concerning the strands except their location and slippage have been provided by Parma Betonila Oy, Nastola factory, the producer of the slabs.

End 1 was in all test the active end.

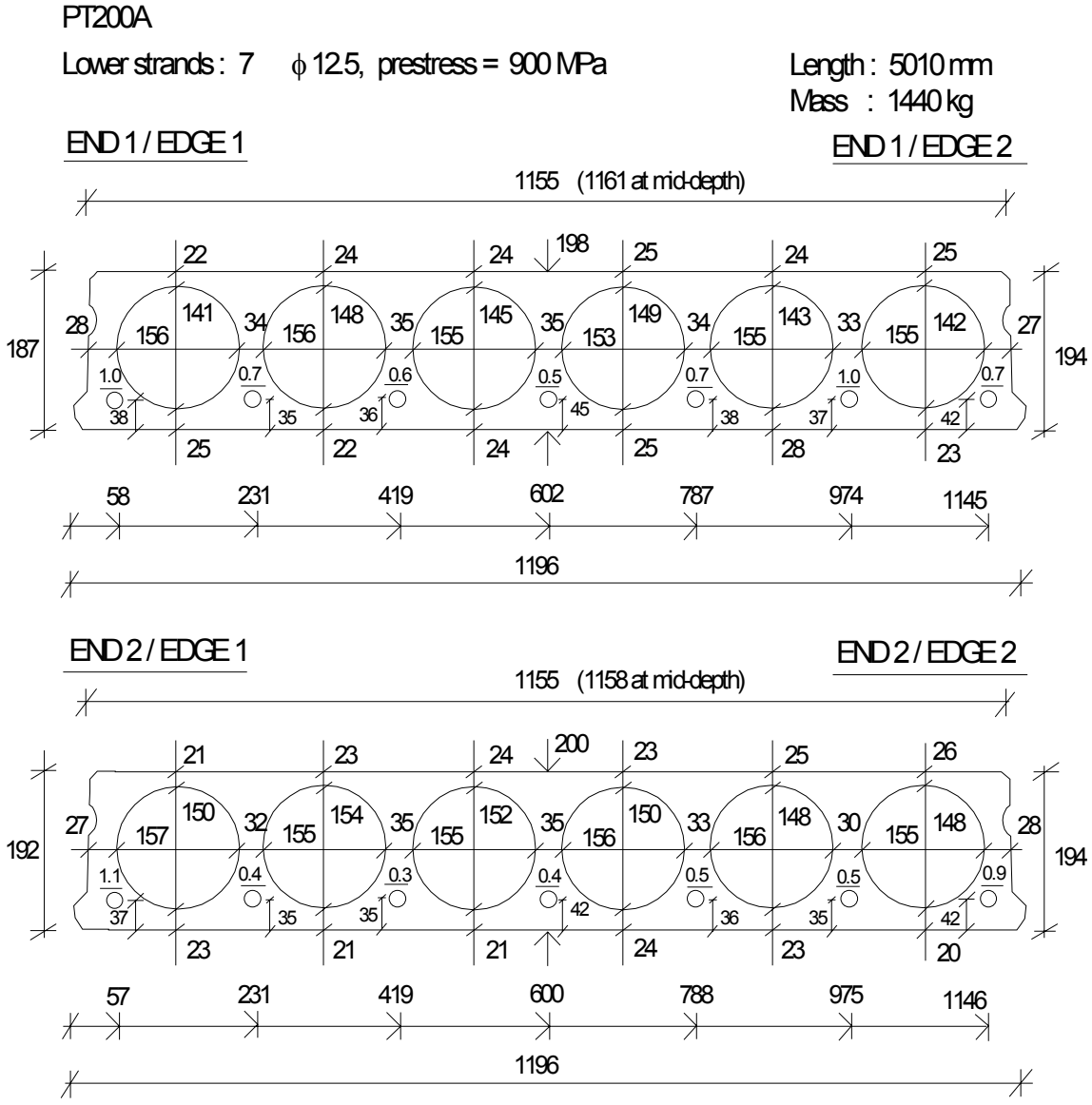

Fig. 1. PT200A.

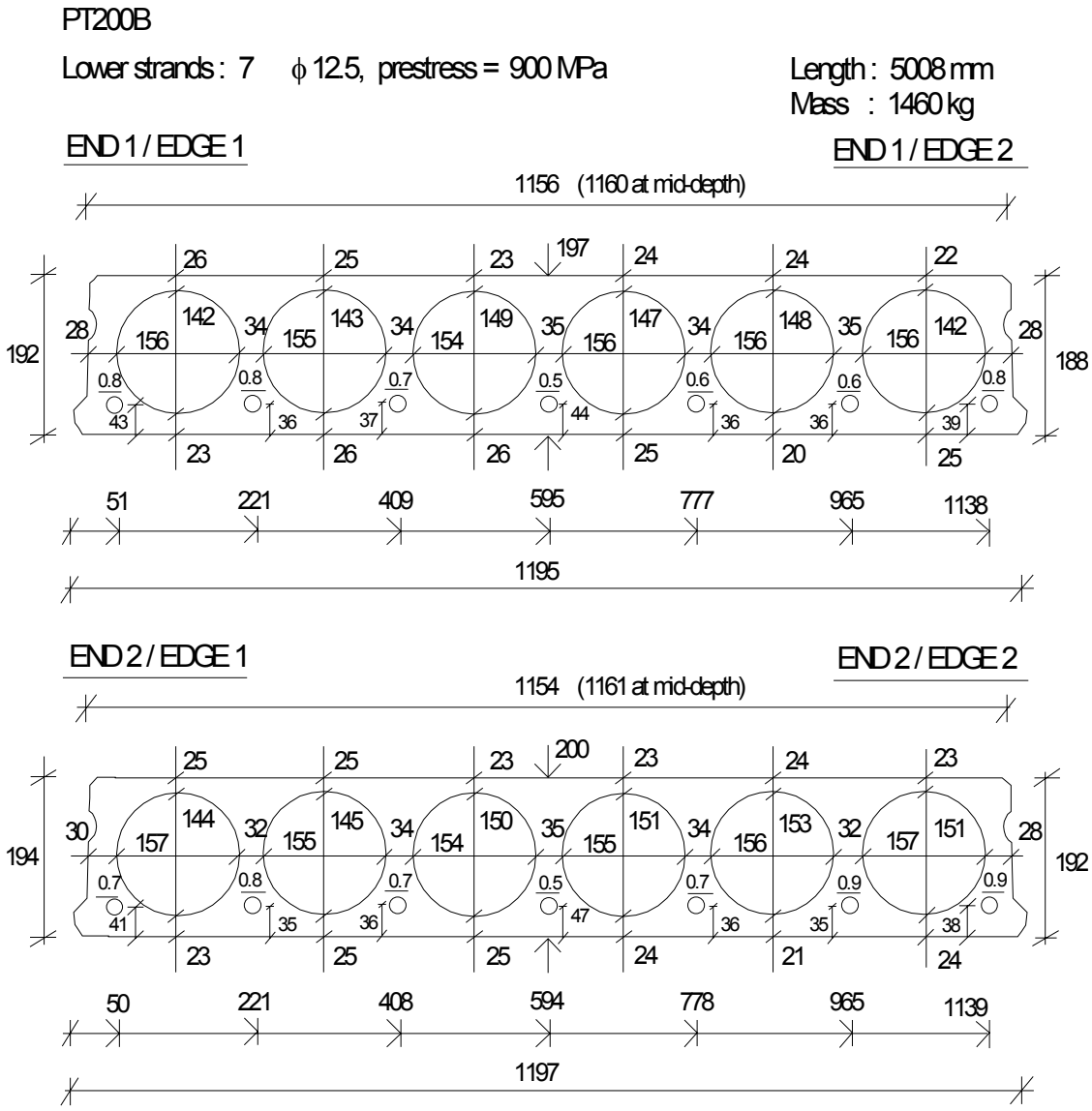
PT200B
Lower strands : 7 ϕ 12.5, prestress = 900 MPa
Length : 5008 mm
Mass : 1460 kg
END 1 / EDGE 1
END 1 / EDGE 2
1156 (1160 at mid-depth)
END 2 / EDGE 1
END 2 / EDGE 2
1154 (1161 at mid-depth)

Fig. 2. PT200B.

PT400A

Lower strands : 7 ϕ 12.5, prestress = 1000 MPa

Length : 7000 mm
Mass : 3610 kg

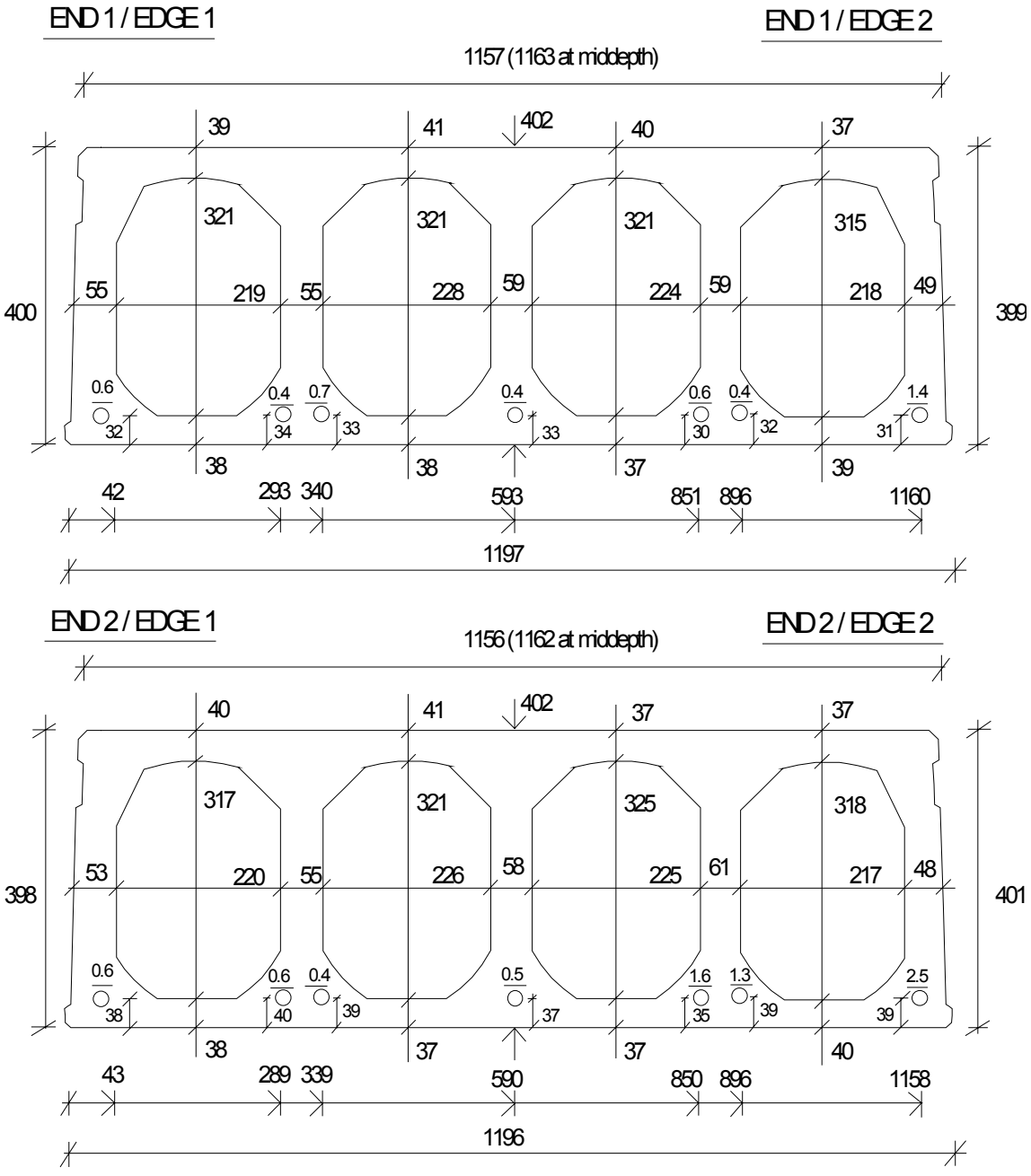

Fig. 3. PT400A.

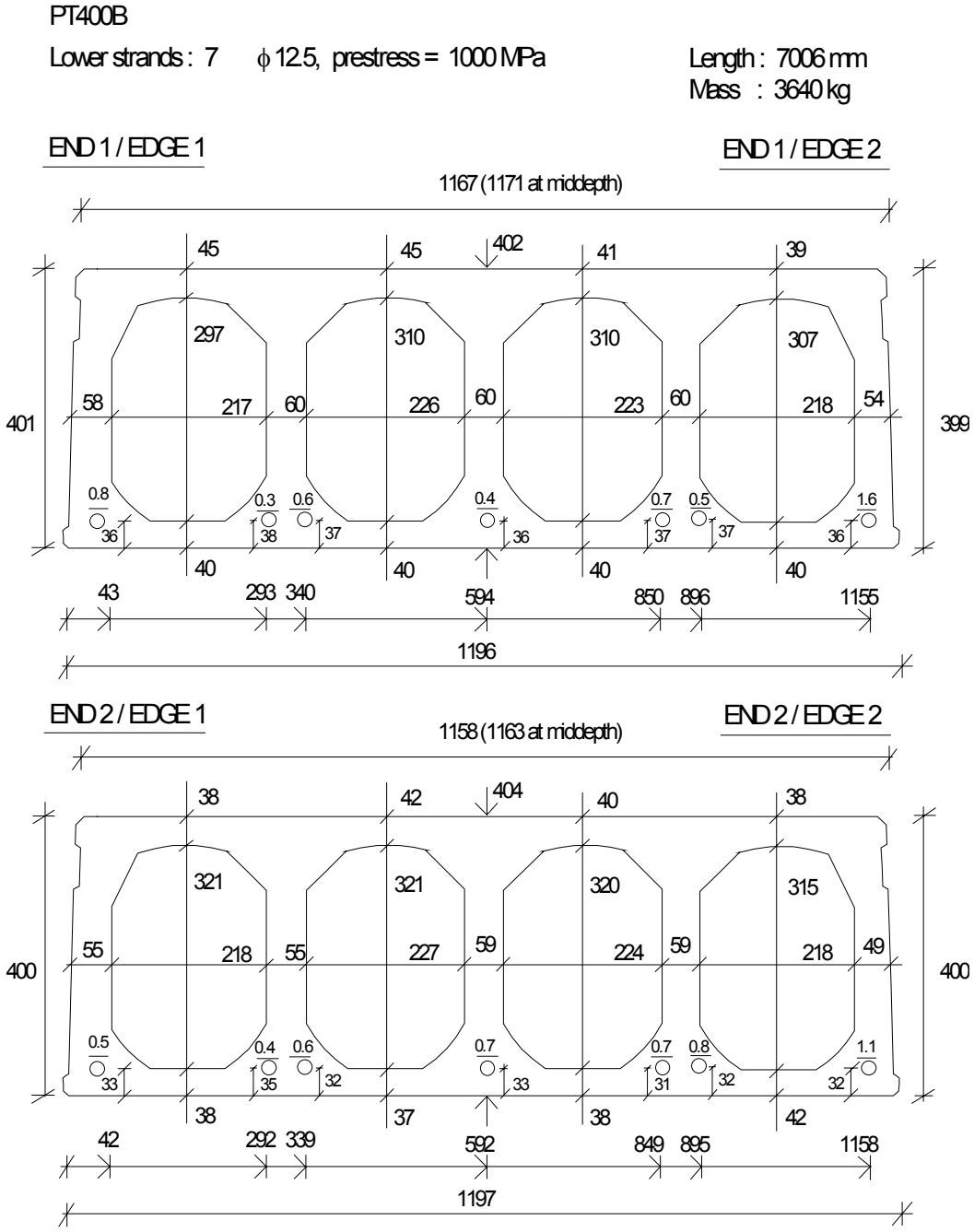
PT400B
Lower strands : 7 ϕ 12.5, prestress = 1000 MPa
Length : 7006 mm
Mass : 3640 kg
END 1 / EDGE 1
END 1 / EDGE 2
1167 (1171 at middepth)
45
45
402
41
39
297
310
310
307
401
58
217
60
226
60
223
60
218
54
399
0.8
36
0.3
38
0.6
37
0.4
36
0.7
37
0.5
37
1.6
36
40
40
40
40
43
293
340
594
850
896
1155
1196
END 2 / EDGE 1
END 2 / EDGE 2
1158 (1163 at middepth)
38
42
404
40
38
321
321
320
315
400
55
218
55
227
59
224
59
218
49
400
0.5
33
0.4
35
0.6
32
0.7
33
0.7
31
0.8
32
1.1
32
38
37
38
42
42
292
339
592
849
895
1158
1197

Fig. 4. PT400B.

Appendix C: Effect of transverse motion at active end on torque

Consider Figs 1 and 2. When the slab rotates around axis O, point C moves to point C'. If the slab is loaded by an actuator, the upper end of which is fixed to point A, see Fig. 2, both the direction and eccentricity of the load are changed. For greater rotations δ the effect of the rotation has to be taken into account when calculating the torque.

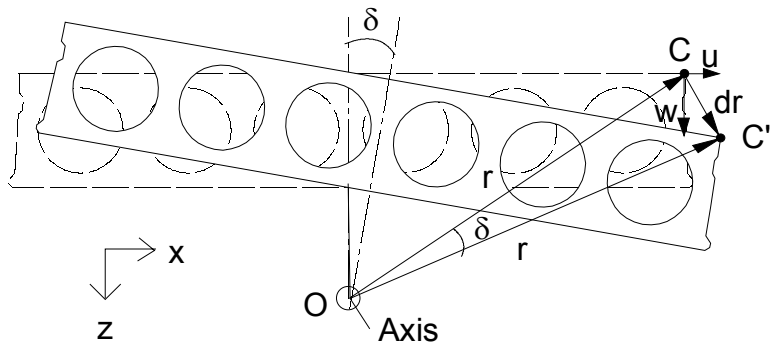

Fig. 1. Rotation of point C at corner of slab and corresponding displacements u and w.

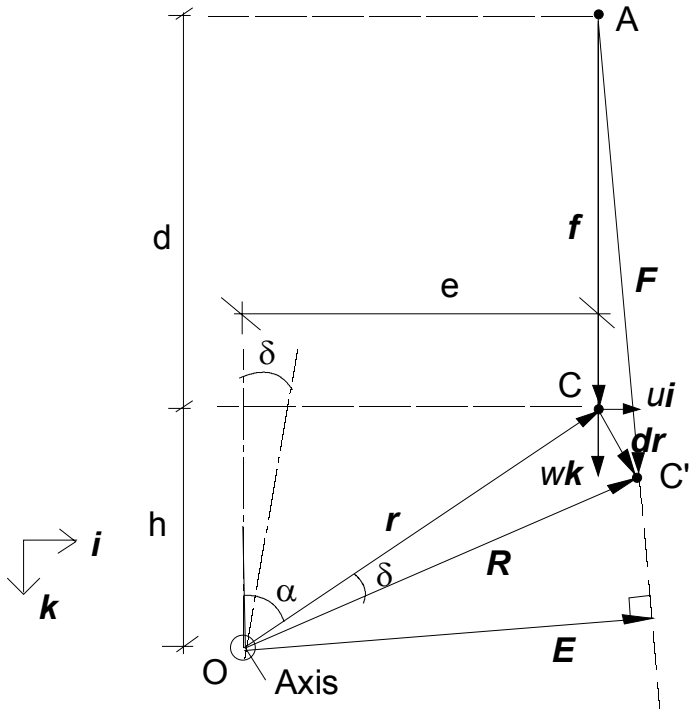

Fig. 2. Notation. d is the initial distance between upper and lower hinge of actuator, e and E are the eccentricity of the load in the initial and displaced state. f and F represent a vector parallel to the actuator force in the initial and displaced state, respectively.

Using the notation expressed in Fig. 2 the perpendicular distance E from rotation axis O to the line passing through A and C' can be calculated. Using the unit vectors ***i*** and ***k*** and omitting the axial motion we get

$$\vec{r} = r\sin\alpha\vec{i} - r\cos\alpha\vec{k} \tag{1}$$

$$\vec{R} = r\sin(\alpha+\delta)\vec{i} - r\cos(\alpha+\delta)\vec{k} \tag{2}$$

$$\vec{R} - \vec{r} = r[\sin(\alpha+\delta) - \sin\alpha]\vec{i} + r[-\cos(\alpha+\delta) + \cos\alpha]\vec{k} = u\vec{i} + w\vec{k} \tag{3}$$

$$\vec{F} = \vec{f} + u\vec{i} + w\vec{k} = u\vec{i} + (d+w)\vec{k} \tag{4}$$

Eccentricity of the load is equal to

$$\left|\vec{E}\right| = \left|\vec{R}\right|\cos\beta = \frac{\vec{R}\cdot\vec{e}}{\left|\vec{e}\right|} \tag{5}$$

where ***e*** is any vector perpendicular to ***F***. E.g.

$$\vec{e} = (d+w)\vec{i} - u\vec{k} \tag{6}$$

is such a vector because $\vec{e}\cdot\vec{F} = 0$. Hence we get

$$\left|\vec{E}\right| = r\frac{(d+w)\sin(\alpha+\delta) + u\cos(\alpha+\delta)}{\sqrt{(d+w)^2 + u^2}} \tag{7}$$

where *r* is the distance from axis of rotation to point C.

From Eq. 8 *u* and *w* are calculated. From Eq. 7 eccentricity of the load is then obtained.

d and *h* are given in Table 1. α is solved from $\tan\alpha = e/h$ where *e* = 300 mm, and $r = (e^2+h^2)^{1/2}$. *u* and *w* are solved from Eq. 3 and *d* is measured. In this way the eccentricity of the actuator load can be calculated from Eq. (7) for all load steps.

Table 1. Measures d and h, see Figs 1 and 2.

	d mm	*h* mm
PT200A	1165	590
PT200B	1730	590
PT400A	1740	790
PT400B	1740	790

Appendix D: Rate of elongation of actuator at active end

The relative torque illustrated in the following figures means the torque at the considered time step divided by the maximum torque observed during the test.

The vibration in the rate of elongation reflects not only the nonlinear response of the loading equipment and the loaded structure but also the inability of the control system to follow the response in sudden changes. On the other hand, the regularity in the behaviour of the applied torque shows that the loading history, with few exceptions, was very close to the aimed one.

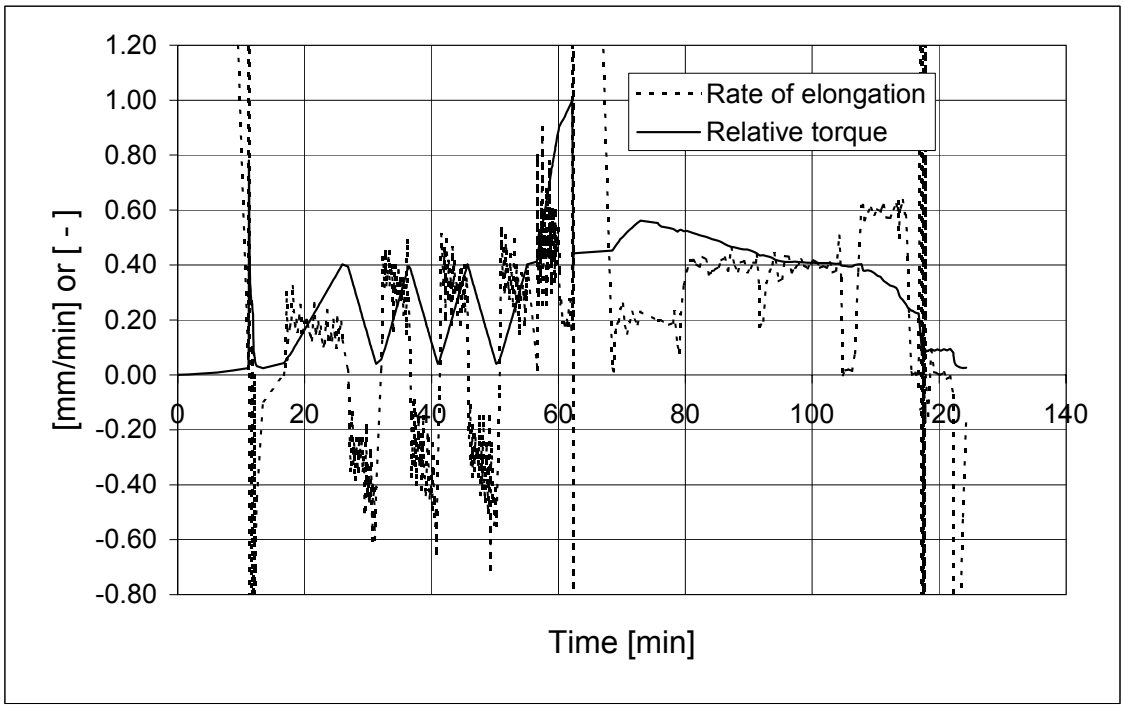

Fig. 1. PT200A.

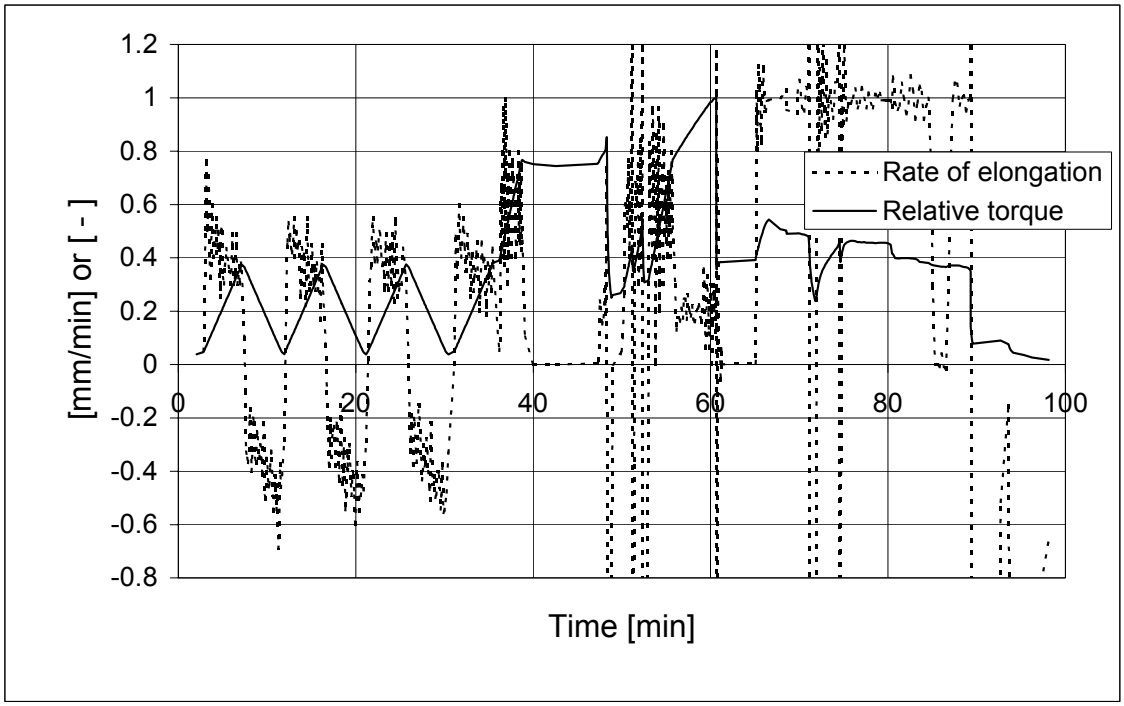

Fig. 2. PT200B.

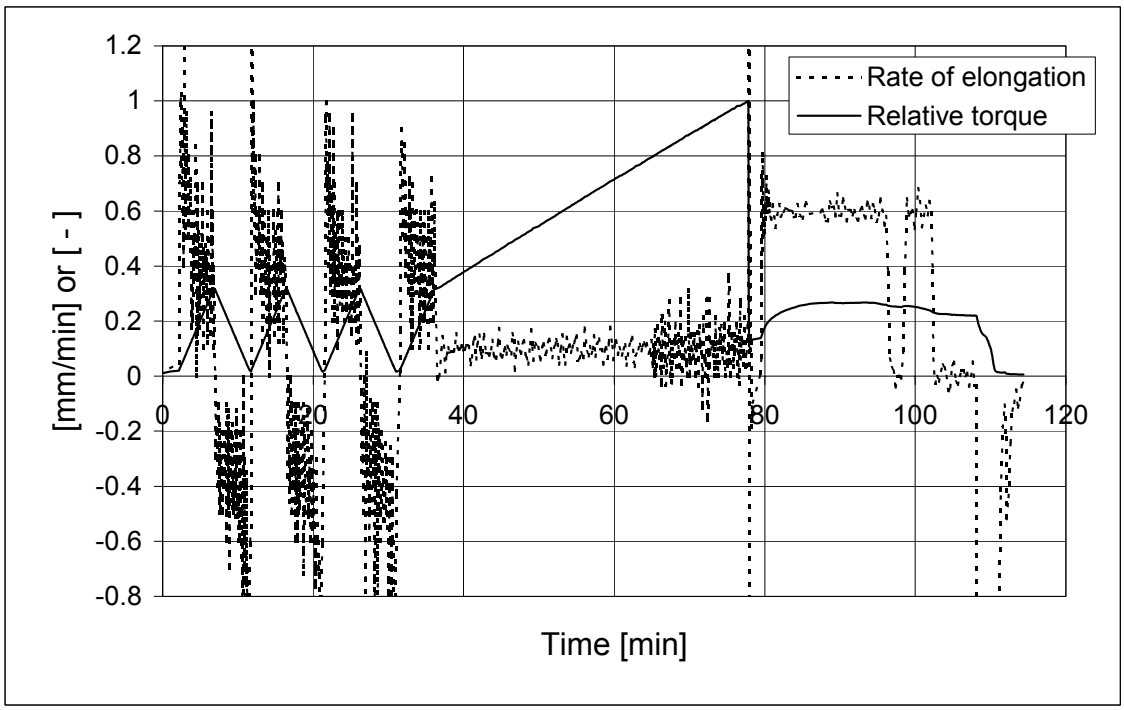

Fig. 3. PT400A.

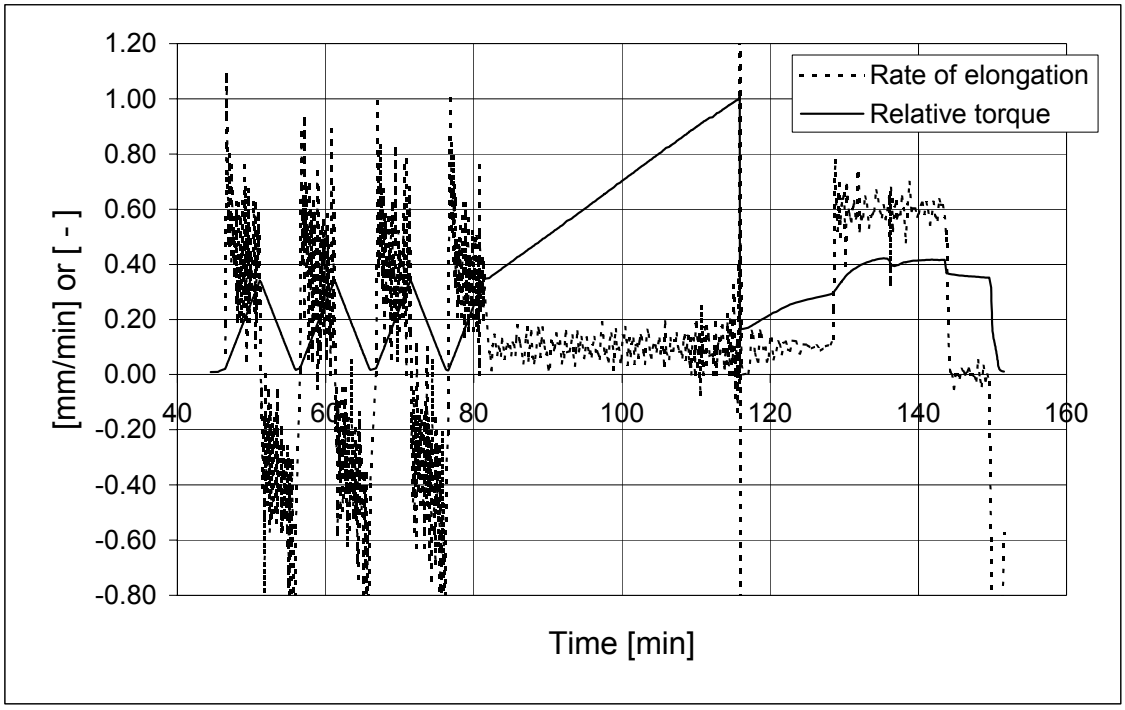
Rate of elongation
Relative torque
[mm/min] or [-]
Time [min]
1.20
1.00
0.80
0.60
0.40
0.20
0.00
-0.20
-0.40
-0.60
-0.80
40
60
80
100
120
140
160

Fig. 4. PT400B.

Published by

Series title, number and
report code of publication

VTT Research Notes 2273
VTT–TIED–2273

Author(s)
Pajari, Matti

Title

Pure torsion tests on single hollow core slabs

Abstract

Four tests on prestressed hollow core slab units were carried out. The slab units, two of them 200 mm and two 400 mm in thickness, were subjected to pure torsion. In all tests the observed failure mode was the same as the predicted one, i.e. cracking of top flange in angle of 45º with the longitudinal axis of the slab unit. Although the failure mode was abrupt, the slab units showed considerable ductility after the failure. None of them collapsed before the test had to be interrupted due to excessive rotation.

For 400 mm slabs the torsional stiffness observed in the tests was close to that predicted by elementary calculation method, but for 200 mm slabs the predicted stiffness was 30% lower than that observed. The predicted torsional resistance was 60% and 70% of the observed resistance for 200 mm and 400 mm slabs, respectively, when the lower characteristic value for the tensile strength of the concrete was used for prediction.

Keywords
shear tests, torsion tests, hollow core slabs, testing, test specimens, load testing, failure loads, concrete, precast, prestressed, structure

Activity unit
VTT Building and Transport, Kemistintie 3, P.O.Box 1805, FIN–02044 VTT, Finland

ISBN			Project number
951–38–6517–7 (URL: http://www.vtt.fi/inf/pdf/)			R2SU00137
Date December 2004	Language English	Pages 29 p. + app. 28 p.	Price -
Name of project Holcotors		Commissioned by EU, Concrete industry, VTT	
Series title and ISSN VTT Tiedotteita – Research Notes 1455–0865 (URL: http://www.vtt.fi/inf/pdf/)		Published by VTT Information Service P.O.Box 2000, FIN–02044 VTT, Finland Phone internat. +358 9 456 4404 Fax +358 9 456 4374	

Four tests on prestressed hollow core slab units were carried out. In the tests the slab units were subjected to pure torsion. In all tests the observed failure mode was the same as the predicted one, i.e. cracking of top flange in angle of 45° with the longitudinal axis of the slab unit. Although the failure mode was abrupt, the slab units showed considerable ductility after the failure. None of them collapsed before the test had to be interrupted due to excessive rotation.

For 400 mm slabs the torsional stiffness observed in the tests was close to that predicted by elementary calculation method, but for 200 mm slabs the predicted stiffness was 30% lower than that observed. The predicted torsional resistance was 60% and 70% of the observed resistance for 200 mm and 400 mm slabs, respectively, when the lower characteristic value for the tensile strength of the concrete was used for prediction.

VTT TIETOPALVELU
PL 2000
02044 VTT
Puh. 020 722 4404
Faksi 020 722 4374

VTT INFORMATIONSTJÄNST
PB 2000
02044 VTT
Tel. 020 722 4404
Fax 020 722 4374

VTT INFORMATION SERVICE
P.O.Box 2000
FIN–02044 VTT, Finland
Phone internat. + 358 20 722 4404
Fax + 358 20 722 4374

ISBN 951–38–6052–3 (URL: http://www.vtt.fi/inf/pdf/)
ISSN 1455–0865 (URL: http://www.vtt.fi/inf/pdf/)